Quantum-defect theory of heats of formation and structural transition energies of liquid and solid simple metal alloys and compounds

J. R. Chelikowsky and J. C. Phillips
Bell Laboratories, Murray Hill, New Jersey 07974
(Received 9 November 1977)

The tables of l-dependent ion-core radii ($l = 0,1,2$) derived from free-ion quantum defects and previously presented by Simons and Bloch are extended to include halogens and the group-I-B metals (Cu, Ag, and Au). From these radii hybridized bond-orbital coordinates with σ and π character are formed. The dual bond-orbital coordinates are used to discuss the structures, uniaxial distortions, and melting points of more than 100 simple binary compounds belonging either to the octet family A^NB^{P-N} with $P = 8$ or to the suboctet family $2 \leq P \leq 6$. Two conclusions emerge: the quantum bond-orbital σ and π dual coordinates describe the physical properties of these materials much more accurately than traditional classical coordinates such as size and electronegativity, and the dual quantum coordinates are equally accurate for octet and suboctet compounds. The success of the quantum coordinates implies that bond charges with σ and π components make important contributions to the structural energies of these materials. The dual coordinate cellular scheme developed by Miedema and co-workers to describe the sign of the heat of formation of liquid and solid metal alloys is examined within the context of orbital, l-dependent ion-core radii. We show that Miedema's original coordinate set is unphysical, but that his inductively revised coordinates which are derived from more than 500 binary phase diagrams are remarkably accurate. Apparent irregularities in the revised coordinates are shown by comparison with the orbital shell model to be correct and the consequence of core shell structure.

I. INTRODUCTION

For many years it has been traditional for physicists to argue that it is not possible to predict the crystal structures of most solids. The difference in equilibrium energies of a given compound in two closely related structures is known from P-T phase diagrams to be very small, often less than 0.1% of the cohesive energy. However, inspection of structural bibliographies[1-4] shows many chemical trends which can be recognized (at least qualitatively) with the aid of the Periodic Table.

This situation can be formulated quantitatively as follows. Structural energy differences are, for the most part, too small to be calculated quantum mechanically, because such calculations require self-consistent crystal potentials of an accuracy beyond the present state of the art. However, if we consider the problem from the point of view of information theory, then the available structural data already contain a great deal of information: about 120 bits, in the case of the A^NB^{8-N} octet compounds. Thus one can reverse the problem, and attempt to extract from the available data quantitative rules for chemical bonding in solids.

The rules that we seek should correspond to the regularities of the Periodic Table. The latter has two coordinates, and these two coordinates take only integral values. To describe chemical bonds therefore we again look for two coordinates, but we allow these coordinates to be nonintegral. Several two-coordinates or dual scaling models of this kind have appeared in the last two decades. It is convenient to refer to them generically as *Mendelyev models*. In contrast to Ising models, X-Y models, Heisenberg models, etc., where the rules of the game are well defined and the aim is to apply the tools of nineteenth century mathematics, Mendelyev models are as yet poorly defined, and considerable physical judgment is required in choosing suitable scaling coordinates.

There are several ways to define scaling coordinates. The coordinates can be extracted from observed properties of the elements, either as isolated atoms or ions, or in the bonded state. The latter approach is more empirical, is more obviously consonant with the small magnitudes of structural energy differences, and is the one adopted by Goldschmit and by Pauling.

The first and most obvious empirical coordinate is the atomic size $r(A)$ for each element A, and tables of atomic radii are available based on metallic and/or ionic structures.[5] The weakness of this coordinate is that spherical atomic packing, by itself, does not suffice to explain the crystal structures of even the simplest compounds, such as the alkali halides.[6] However, this classical coordinate is often used in discussions of crystal chemistry, and it does exclude from consideration many "unreasonable" structures which are never formed.

The second coordinate with a sound empirical basis is Pauling's elemental electronegativity $X(A)$ which is derived from heats of formation.[5] Again

this coordinate, which is related to work functions, is classical in character. It has no directional aspects and, like atomic radii, is not well suited to discussing structures where covalent bonding is important.

The two classical coordinates, atomic size and electronegativity, were used by Darken and Gurry[7] to construct two-dimensional graphs to analyze intermetallic alloy solubilities at small concentrations. This method was relatively successful (75%) in predicting solubility trends. However, the first major breakthrough using dual chemical coordinates came with the classification of crystal structures by Mooser and Pearson.[8] They restricted their attention to simple binary compounds (or pseudobinary compounds such as the chalcopyrites). The coordinates they used consisted again of Pauling's classical electronegativity scale, but the other coordinate involved the average principle quantum number $\bar{n} = \frac{1}{2}[n(A) + n(B)]$. With these coordinates they were quite successful (90%–95%) in separating the fourfold and sixfold coordinated octet compounds. In addition they were also successful in separating many transition metal compounds of the form TB^N (T is a transition metal and B^N is a nontransition metal with N valence electrons: $3 \leq N \leq 6$). Note that the principal quantum number $n(A)$ is more nearly linearly independent of $X(A)$ than is the atomic radius $r(A)$. The Mooser-Pearson coordinates have some quantum-mechanical character, but at the same time they retain part of the original digital metric of the periodic table itself. The Mooser-Pearson coordinates constitute a simple, almost classical, shell model.

For the special case of the octet compounds Phillips and Van Vechten introduced[6,9] two fully quantum-mechanical nonintegral coordinates. These were the average covalent energy gap E_h and the average ionic energy gap C, both of which were derived from the bond lengths and dielectric constants of the compounds. They were able to separate exactly the fourfold and sixfold coordinated $A^N B^{8-N}$ compounds. Moreover, both their bond variables have the dimensions of bond energy, this appears desirable for structural plots which depend on differences of cohesive energies. Unfortunately, while their separation was exact, their method is applicable only to fully bonded cubic crystals [i.e., no lone pair or unpaired (metallic) electrons].

In this paper we shall discuss a recent classification scheme first developed by St. John and Bloch[10] based upon orbitally dependent radii as determined by a Pauli-force model potential developed by Simons and Bloch.[11–13] The coordinate scheme of St. John and Bloch stands out as a significant improvement over previous classifications for several reasons. First, the radii used in their scheme may be incorporated into an electronegativity scale which contains orbitally dependent contributions. This implies that it is more refined than classical isotropic approaches.[7,8] For example, it lends itself to a discussion of structural variations in chemical hybridization which is not feasible with other scales. Second, St. John and Bloch, using as coordinates this scale and a structural parameter based upon a combination of the Simons-Bloch orbital radii,[14] were able to separate exactly hcp, fcc, bcc, and "covalent" structures among the elements. Further, when appropriate σ and π combinations of orbital radii were used as coordinates they were able to separate exactly the graphite, zinc-blende, wurtzite, rocksalt, and cesium chloride structures of the octet binary compounds. Third, their coordinates, unlike the Mooser-Pearson scheme, are derived entirely from quantum variables, yet vary smoothly across the periodic table. This is a significant requirement for any coordinate scheme to be used in crystal structure classification. [One of the major drawbacks of the Mooser-Pearson $\bar{n}$ coordinate is that it is of a digitalized form. Thus it cannot be expected to separate fine differences or to account for smoothly varying properties (such as c/a ratios). Nevertheless it should be noted $\bar{n}$ is of a quantum nature and does properly account for gross chemical trends such as the increasing metallicity of the group-IV elements with $\bar{n}$.] Finally, and most significantly, the coordinates used by St. John and Bloch have been applied to suboctet binary crystals such as CaHg, KSi, LiAl, and CsAu. These fractionally bonded nontransition metal compounds also lend themselves to a nearly exact separation using the *same* coordinate scheme as for the octet binaries.[15] As previously noted, the dielectric theory is not suited to such systems and the Mooser-Pearson scheme has been shown to be unsuccessful in this case.[15]

Although the Bloch-Simons orbital radii are very general, their physical significance as ion-core coordinates leaves us unprepared for their success in forming bond-orbital coordinates for neutral atoms. Thus in discussing the Bloch-Simons radii and the St. John–Bloch scheme we first review (in Sec. II) the basic concepts and the definitions used to formulate the radii. In this section we also explicitly tabulate the radii and display the trends of the radii across the Periodic Table. We also discuss the $l = 2$ trends of the radii for all nontransition elements. In particular, we find it necessary to modify the St. John–Bloch electronegativity scale because fo the altered $l = 2$ radii. In Sec. III the physical meaning of bond-orbital coordinates is brought out by comparing the St. John–Bloch coordinates to other proposed coordinates: those

of Mooser and Pearson and those of Phillips and Van Vechten.

In Sec. IV we review previous work on the octet and suboctet binary compounds. We extend these results to include some binaries not included in the St. John–Bloch plots such as the noble metal (i.e., Cu, Ag, Au binaries). In the suboctet group we discuss melting points and the internal structure of the CrB family and contrast our results with trends based upon the Mooser-Pearson coordinates. In Sec. V we discuss the c/a ratios of wurtzite compounds and structural trends in the ternary compounds $A^{II}B^{IV}C_2^V$. In Sec. VI we discuss the two isotropic parameters introduced by Miedema, Boom, and de Boer and show that for simple metals these parameters can be expressed very accurately in terms of orbital radii. In Sec. VII we review some of our conclusions and discuss the implications of our success for the systematic development of nonlocal pseudopotential theory.[16]

II. DEFINITIONS AND PHYSICAL CONTENT OF ORBITAL RADII

The basis of the bond-orbital coordinate system used by St. John and Bloch rests on orbital ionic radii as determined by a pseudopotential for the free ion. Simons, using a potential first introduced by Fues,[17] wrote the ionic potential as follows:

$$V(r) = -\frac{Z}{r} + \sum_{l=0}^{Z} \frac{\hat{l}(\hat{l}+1) - l(l+1)}{2r^2} P_l \qquad (1)$$

in atomic units, where Z is the net core charge, P_l is a projection operator which projects out the lth component of angular momentum, and $\hat{l}$ is an l-dependent parameter. This potential replicates only the valence states and represents, away from the nucleus, the one-valence electron ion potential. The principal advantage of (1) is that it yields an exact solution to Schrödinger's equation and thus eigenvalues and eigenvectors are easily obtained. According to the results of Fues, the eigenvalues of (1) may be written

$$E_{n,l} = -Z^2/2(n + \hat{l} - l)^2 \ . \qquad (2)$$

This result may be interpreted as a Rydberg series with an l-dependent quantum defect. To obtain values for this defect $\delta_{n,l}$ resort may be made to experimental spectroscopic data for the one-valence electron system.[18,19]

It is probably worth contrasting the l-dependent nature of (2) with the free atom, where l is a good quantum number and the quantum defect is associated with n. For bonded electrons $\delta_{n,l}$ is interpreted as entirely an l defect because l is no longer a good quantum number in solids. In particular, l mixing or chemical hybridization occurs in solids (e.g., sp^2, sp^3), whereas n remains almost a good quantum number. We sometimes call this the orbital shell model.

Bloch and Simons[13] first made use of this principle of maximal hybridization in the analysis of chemical trends among the elements. They expressed the trends in terms of radii which they defined as

$$r_l = \hat{l}(\hat{l}+1)/Z \ . \qquad (3)$$

These radii represent the positions of the radial maxima of the ionic eigenfunctions resulting from (1). They are also a factor of 2 larger than the classical turning points of (1) at $V=0$. The classical turning radii change very little on going from the ion to the neutral atom, because very little valence charge accumulates inside radii. The radial maxima of the neutral atom eigenfunctions, however, are considerably greater than those of the hydrogenic ions. Moreover, the classical radii are more significant physically[16] as we are interested in examining *potential* differences near $E = E_F$ (in the solid) or $E = 0$ (isolated atom or ion) and not wave functions. However, none of the results discussed here would be altered by rescaling r_l by a factor of 2 and thus we shall retain the Simons original definition, Eq. (3).

St. John and Bloch[10] showed that a successful classification scheme for octet binaries resulted if the following bond-orbital coordinates were employed:

$$r_\pi = r_\pi^A + r_\pi^B \ , \quad r_\sigma = r_\sigma^A - r_\sigma^B \ , \qquad (4)$$

where $r_\sigma^\alpha = r_s^\alpha + r_p^\alpha$ and $r_\pi^\alpha = r_p^\alpha - r_s^\alpha$. These bond-orbital coordinates play a role analogous to $\bar{n}$ and ΔX of Mooser-Pearson and to E_h and C of Phillips and Van Vechten. Phillips[16] has presented a physical interpretation of these coordinates in which r_σ^α corresponds to s-p σ hybrids on atom α, while r_π^α corresponds to p^2-sp hybrids, i.e., r_π^α measures the strength of π bonding over and above the σ bond strength. This argument is based upon traditional chemical explanations. However, this does not imply that classical hybridized free-atom orbitals present a method for describing all the valence charge density. If this were the case, we would use orbital radii associated with the *atomic* valence orbitals and not the *ionic* radii of Simons and Bloch. The quantum-mechanical interpretation of the Bloch-Simons orbital shell radii, therefore, must be sought in a pseudopotential context.[16]

In order to study the physical shell content of orbital shell coordinates we first extended the results of Simons. In particular, using spectroscopic data[19] we extended his earlier work to include halogens, I-B metals, and $l=2$ trends in the radii. Our results are presented in Table I and displayed

TABLE I. Orbitally dependent ionic radii as defined by Bloch and Simons [see Eq. (3)]. Radii are given in atomic units. Radii listed in parentheses have been obtained by extrapolation. In addition to the radii, the electronegativity for each element is tabulated as defined by Pauling, St. John–Bloch, and Phillips. The St. John–Bloch scale has been modified from the original definition as discussed in the text.

Element	r_s	r_p	r_d	X_{Pauling}	$X_{\text{St. John–Bloch}}$	X_{Phillips}
Li	0.93	1.88	5.99	1.0	0.97	1.00
Na	1.02	2.36	5.95	0.9	0.89	0.72
K	1.36	2.76	5.29	0.8	0.77	0.79
Rb	1.45	2.95	4.89	0.8	0.74	0.66
Cs	1.62	3.18	3.96	0.7	0.72	0.64
Be	0.63	0.93	3.00	1.5	1.49	1.50
Mg	0.86	1.43	2.92	1.2	1.15	0.96
Ca	1.22	1.87	1.52	1.0	1.07	0.91
Sr	1.36	2.09	1.74	1.0	0.98	0.83
Ba	1.55	2.34	1.71	0.9	0.92	0.79
Cu	0.43	1.61	5.89	1.9	1.53	0.79
Ag	0.45	1.66	5.90	1.9	1.48	0.57
Au	0.26	1.40	5.87	2.4	2.22	0.64
Zn	0.64	1.22	3.06	1.6	1.36	0.91
Cd	0.71	1.32	3.18	1.7	1.27	0.83
Hg	0.60	1.26	3.24	1.9	1.39	0.79
B	0.48	0.62	2.00	2.0	2.00	2.00
Al	0.74	1.08	1.92	1.5	1.40	1.18
Ga	0.66	1.04	2.15	1.6	1.46	1.13
In	0.76	1.17	2.31	1.7	1.32	0.99
Tl	0.69	1.16	2.41	1.8	1.37	0.94
C	0.38	0.47	1.50	2.5	2.50	2.50
Si	0.66	0.89	1.42	1.8	1.64	1.41
Ge	0.64	0.92	1.68	1.8	1.59	1.35
Sn	0.76	1.07	1.87	1.8	1.40	1.15
Pb	0.72	1.09	1.98	1.8	1.41	1.09
N	0.32	0.38	1.20	3.0	2.99	3.00
P	0.59	0.76	1.13	2.1	1.87	1.64
As	0.62	0.83	1.41	2.0	1.71	1.57
Sb	0.72	0.97	1.56	1.9	1.52	1.31
Bi	0.72	1.02	1.78	1.9	1.46	1.24
O	0.28	0.32	1.00	3.5	3.49	3.50
S	0.53	0.66	0.94	2.5	2.10	1.87
Se	0.59	0.76	1.21	2.4	1.84	1.79
Te	0.69	0.89	1.35	2.1	1.62	1.47
Po	(0.71)	(0.98)	(1.67)	2.0	(1.50)	···
F	0.24	0.27	0.86	4.0	3.99	4.00
Cl	0.49	0.59	0.80	3.0	2.33	2.10
Br	(0.55)	(0.74)	(1.15)	2.8	(1.93)	2.01
I	(0.66)	(0.85)	(1.37)	2.5	(1.67)	1.63
At	(0.69)	(0.90)	(1.65)	2.2	(1.56)	···

in Figs. 1–3. In the case of the heavier halogens, e.g., I and At, spectroscopic data are not available. In those cases the values of r_l were obtained by extrapolation across the row and down the column of the Periodic Table. Unlike the suggestion of Bloch and Simons[13] we have *not* made the approximations $\hat{l}(l=1)=1$ for all first row elements and $\hat{l}(l=2)=2$ for elements other than the alkali and alkali-earth metals. In most cases this approximation is a valid one; however, in a few cases, e.g., Ge and Si, the $l=2$ radii are of crucial importance.

A remarkable feature of the orbital shell radii, first recognized by St. John and Bloch,[10] is that they can be used to define an orbital electronegativity scale $\tilde{X}(A)$. This scale generalizes the Pauling electronegativity scale $X(A)$. Pauling defined $X(A)$ qualitatively as "the power of an atom in a bonded state to attract electrons to itself." Quantitatively the parameters $X(A)$ were derived in two ways:

(i) By demanding that for the first period elements

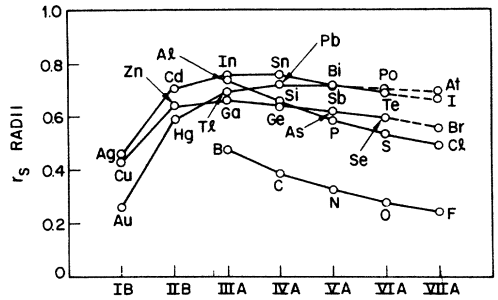

FIG. 1. $l=0$ Bloch-Simons radii in atomic units as defined by Eq. (3). Note the effect of the closed d shell in the (Cu, Ag, Au) series as evidenced by the nonmonotonic behavior of the radii.

$2X(A)=Z(A)+\text{const}$, where $Z(A)e$ is the ion-core charge, e.g., $Z(\text{C})=4$, $Z(\text{N})=5$. The justification for this procedure is that in the first period the atomic ground states can be described by $2s^{m_0}2p^{n_0}$ and the hybridized states by $2s^m2p^n3d^p$ with $m_0+n_0=Z$ and $p\ll 0.1$, i.e., the admixture of $3d$ states into $2s$-$2p$ hybridized bonds is negligible. Also for covalent and metallic bonds $m+n+p=Z+\delta$ where δ is usually much larger than p but is still of order a few tenths or less in most cases. The condition $\delta>p$ is not usually satisfied for chemical bonds involving other elements where $p>0.1$, e.g., $3s3p3d$ hybridized states.

(ii) By assuming that heats of formation $\Delta H(AB)$ per resonating bond were given by $[X(A)-X(B)]^2$ in eV.

Because the orbital shell radii r_l refer to isolated ions, only condition (i) can be used to characterize an electronegativity scale based on them. Nevertheless, this is a severe condition and in spite of the intuitive appeal of the St. John–Bloch definition

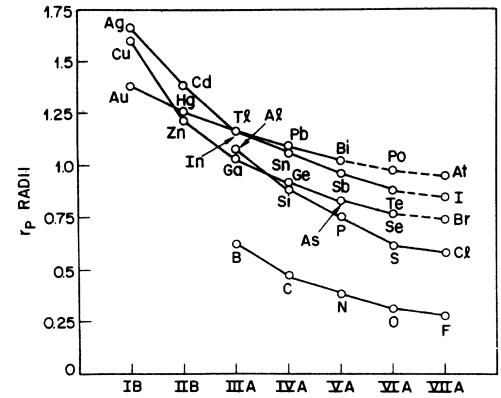

FIG. 2. $l=1$ Bloch-Simons radii in atomic units as defined by Eq. (3). Unlike the $l=0$ radii (Fig. 1), the closed d shell in the (Cu, Ag, Au) series has a relatively weak influence on the $l=1$ radii.

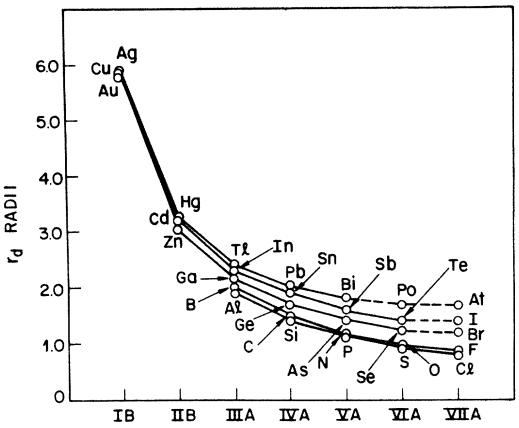

FIG. 3. $l=2$ Bloch-Simons radii in atomic units as defined by Eq. (3). Note the large influence of the closed d shell for the noble metals (Cu, Ag, Au).

$$\tilde{X}(A)=a\sum_{i=0}^{2}\frac{1}{r_i(A^{+Z})}+b\ , \tag{5}$$

it is by no means obvious why $\tilde{X}(A)$ satisfies condition (i) above so well.

A partial explanation for the success of (5) for first period elements can be given as follows. By fitting the values of r_i given in Table I to a Laurent series in Z we find that for the first period elements

$$1/r_0=\tfrac{1}{2}Z+0.62-0.05/Z\ , \tag{6}$$

$$1/r_1=\tfrac{1}{2}Z+0.15-0.13/Z\ , \tag{7}$$

$$1/r_2=\tfrac{1}{6}Z\ . \tag{8}$$

For an average value of $Z=4$, the correction terms in Z^{-1} in (6) and (7) are of order 1% of the terms in Z. Substitution of (6)–(8) in (5) requiring (i) gives $a=\frac{6}{13}$. However, the best fit is given by $a=0.423$ and $b=0.224$ [in order to make $\tilde{X}(C)=2.50$ in agreement with Pauling].

The large Z limits of (6)–(8), and especially (6), can be obtained by the quantum defect method. In the limit $Z\to\infty$ the quantum defects $\delta_{nl}\to 0$, for $(nl)=(2s)$, $(2p)$, and $(3d)$. In particular, $\hat{l}_0=1+\delta_{2s}$, and so from (3),

$$r_0=\hat{l}_0(\hat{l}_0+1)/Z=(1+\delta_{2s})(2+\delta_{2s})/Z\to 2/Z\ . \tag{9}$$

From this discussion one might conclude that $\hat{l}(l)$ is merely a convenient way of relabeling the quantum defects δ_{nl}. Then one might attempt to calculate δ_{nl} by expansion in a series in Z^{-1}. However, when this is done, the constant term on the right-hand side of (6) is overestimated by a factor of 20 when it is obtained by first-order perturbation theory using hydrogenic $2s$ wave functions and the $1s$ core potential as the perturbation. The well-known

reason for this is that the $2s$ state must be orthogonalized to the $1s$ states and this orthogonalization is significant except for very large Z ($Z \gg 10$, as the perturbation calculation shows). Thus the actual correction terms in (6) are small because of the cancellation theorem.[18] It is one of the objectives of Mendelyev models to avoid calculation of δ_{nl}, on the grounds that the accuracy of such calculations is usually justified in any event by reference to experimental spectra or other empirical sources.

Because the leading terms in (6)–(8) are all proportional to Z, and because the correction terms in Z^{-1} are so small, condition (i) does not determine $\tilde{X}$ uniquely. Indeed $\tilde{X}$ could also be defined as

$$\tilde{X} = a \sum_{l=0}^{2} \frac{g(l)}{r_l} + b \ , \tag{10}$$

and condition (i) would still be satisfied for a wide choice of positive values of $g(l)$.

The choice of $g(l) = 1$ made by St. John and Bloch can be justified partially, as they note, by comparing $\tilde{X}$ thus defined with X_{Pauling} and X_{Phillips}. For most nontransition elements $2\tilde{X} = X_{\text{Pauling}} + X_{\text{Phillips}}$. Because X_{Pauling} is based to a large extent on molecular heats of formation (where hybridization is minimal) and X_{Phillips} is based on fully hybridized crystalline sp^3 bonds, the choice $g(l) = 1$ seems judicious. However, for certain structural families other weighting factors may be appropriate [e.g., in layer compounds, $g(0) = 1$ and $g(1) = 2$ may be more successful].

One of the classical tests for an electronegativity scale, first proposed by Gordy and Thomas,[20] is the extent to which the scale correlates linearly with the work functions $\phi(A)$ of elemental metals. If $X(A)$ is defined thermochemically, in the manner of Pauling, then one might not expect the correlation to be excellent. Moreover, in practice the measured values of $\phi(A)$ show substantial scatter (of order 0.5 eV) because of variations in surface preparation. Nevertheless, thermochemical data can be used as a starting point for such a correlation as discussed below.

A refined thermochemical treatment of the heats of formation ΔH of metallic alloys and compounds (both solid and liquid) has been given by Miedema, Boom and, deBoer.[21,22] In addition to the negative contribution to ΔH from $(\Delta\phi^*)^2$, where ϕ^* is an electronegativity parameter, they include a positive contribution related to $(\Delta n)^2$, where $n = n(r_{\text{WS}})$ is the electron density at the Wigner-Seitz or atomic radius. Their positive boundary contribution is not the same in principle or in practice as a size-mismatch energy, for it is similar in solid and liquid alloys. Their model is specific to metals (it would not apply to ionic crystals, where size mismatch is important) and their empirically adjusted values of ϕ^* are similar to measured values of ϕ. However, their table of values of ϕ^* for 26 nontransition and 27 transition metals, based on the phase diagrams of 481 binary systems, probably constitutes one of the better semiempirical sources of values which can be compared to proposed electronegativity scales. The application of (10) to the Miedema scales is discussed in detail in Sec. VI.

In Figs. 1–3 the r_l radii are displayed across the periodic table. There are several specific observations which can be made with respect to these figures. If we compare the r_s and r_p radii we note that for both the first row is separated from the second and higher rows; this trend is not observed for the r_d radii. For example, in the case of C we have $r_s = 0.38$, $r_p = 0.47$, and $r_d = 1.50$ while in the case of Si we have $r_s = 0.66$, $r_p = 0.89$, and $r_d = 1.42$. Part of the reason for the large separation between the first and second rows is the lack of $n = 1$ core states to which the $n = 2$ valence states must be made orthogonal. In pseudopotential language this results in reduced cancellation of valence states as there exist no $1p$ core states and only $1s$ state to cancel the strong core potential. This makes the first row atoms abnormally small as compared to those from the higher rows, and lends them unique character. We also note the relative s-p cancellation is of considerable importance. This is particularly true of the group-IV elements. For example, in going down the column the s-p separation increases. There is even an inversion $r_s(\text{Sn}) > r_s(\text{Pb})$ which results in the failure of Pb to form sp^3 hybrids as the promotion energy from s^2p^2 to sp^3 becomes too large. Thus C forms in the diamond lattice, but not Pb.

With respect to r_d similar observations may be made. In the first two rows, no d states exist within the core region. Therefore, no d cancellation can occur for the first two rows. This results in the smaller and nearly identical values for r_d in the first two rows in contrast with the higher rows. As an example, in C, Si, Ge, and Sn we have $r_d = 1.50$, 1.42, 1.68, and 1.87, respectively.

As we go across the rows we expect r_l to contract as the core charge increases. This is true for the cases of r_p and r_d, but not for r_s (with the exception of the first two rows). The rather rapid decrease of r_d especially for the sequence I-B–II-B–III-A is a reflection of the rapid contraction of the just filled d shell. The d-shell core in Cu is highly polarizable and contributes significantly to the cohesive energy. The variation of r_s is also quite interesting in that the radii appear to correlate exceptionally well with Pauling's atomic radii.[5] For example, the maximum of Pauling's radii in

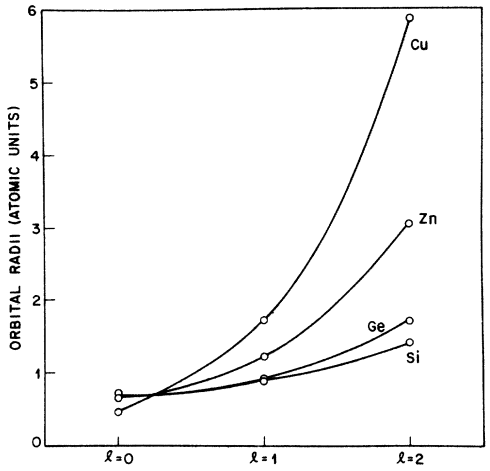

FIG. 4. Bloch-Simons radii as a function of l for selected elements. Note the effect of the closed $3d$ shell on the $l=2$ radii for the Cu-Zn-Ge sequence. The chemical differences between Si and Ge can be traced to the $l=2$ radii.

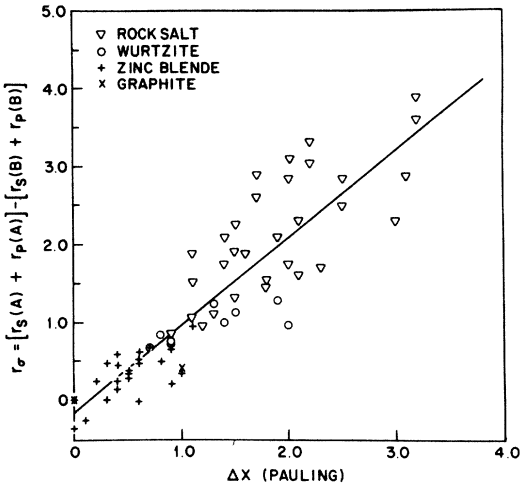

FIG. 5. St. John–Bloch coordinate r_σ vs the electronegativity difference ΔX from Pauling for 67 octet binary compounds $A^N B^{8-N}$. The good correlation occurs, in part, because both $r_s + r_p$ and X correlate with atomic size.

the Ag-Cd-In-Sn-Sb sequence occurs at In, which is also the case for r_s.

The usefulness of these radii in predicting chemical trends among the elements is graphically illustrated in Fig. 4. Here we display the changes with l of the radii for the elements Cu, Zn, Ge, and Si. In the case of Cu where the $3d$ shell has just filled the difference between r_s and r_p with respect to r_d is quite significant as compared to Ge. Note also that the exceptionally small value of r_s in Cu is an extrapolation of the r_d-r_p trend, i.e., the r_l values are indeed analytic functions of l. The highly polarizable nature of Cu, or its "softness" as a noble metal compared to Ge, can be described by an index by making use of derivatives of such curves [e.g., $(r_2 - r_0)/(r_2 + r_0)$]. The relative smoothness of the transition from Ge to Cu is also encouraging. This regularity of change, in part, justifies the use of r_d as an index of the relative d-state influence upon the chemical properties. As we have pointed out previously, it is interesting to observe the trends between Si and Ge. Si and Ge have almost identical r_s and r_p values, so that it is r_d which separates them chemically. In fact, most of the chemical differences existing between Si and Ge such as the cohesive energies have been related to the metallizing effect of the d-core level.[23]

III. COMPARISON OF CHEMICAL COORDINATES

In Figs. 5–8 we compare the Bloch–St. John coordinates with those of Mooser-Pearson (MP) and with those of Phillips–Van Vechten (PVV). As we have seen previously, the St. John–Bloch (SB) coordinates r_σ and r_π might correspond to the MP coordinates ΔX and $\bar{n}$ and to the PVV coordinates E_h and C. In Fig. 5 we display the electronegativity differences of Pauling versus the r_σ parameter of SB. The usefulness of Pauling's scale as a coordinate is quite apparent as it dictates trends in ionicity (although it does contain some deficiencies as mentioned above). The bond-orbital coordinate r_σ measures this property by correlating to some degree the relative sizes of the ions. In Fig. 5 we have plotted points taken from the 67 crystal structures corresponding to the octet group. An explicit list of the structures displayed and values of C and E_h may be found in Ref. 9. Overall, the correlation is fairly good, with the widest scatter occurring for the rocksalt structure. The electronegativity scale of Pauling we note is not capable alone of separating the structures. In particular, near $\Delta X = r_\sigma \approx 1$ there is considerable mixing of rocksalts, wurtzites, and zinc blendes. Another interesting trend is that the least-squares-fitted line displayed in Fig. 5 intercepts quite near $r_\sigma = 0$, as it should if $r_\sigma \sim \Delta X$. The linear fit in Fig. 5 yields

$$r_\sigma = 1.12\Delta X - 0.15 \,, \tag{11}$$

where r_σ is in a.u. and ΔX is as given by Pauling.[5]

In Fig. 6 we display a similar plot of r_π vs $\bar{n}$. MP chose this coordinate because it appeared to be a good measure of the directional character of the bonds formed between an atom with atoms of its own kind. As $\bar{n}$ increases, they point out, the atomic orbitals involved in bond formation, and hence the bonds themselves, gradually lose their direction properties. (The increase in metallicity

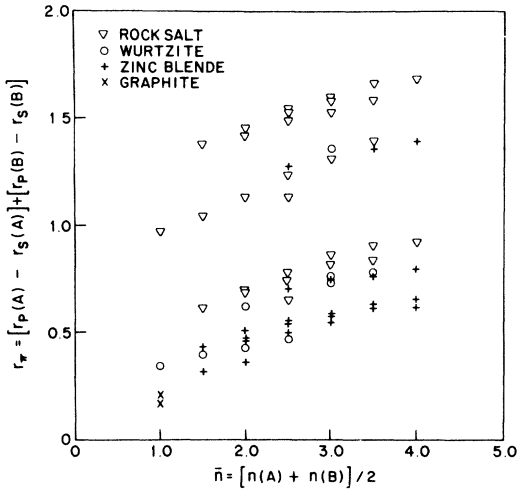

FIG. 6. St. John–Bloch coordinate r_π vs the Mooser-Pearson coordinate, the principal quantum number $\bar{n}$ for 67 octet binary compounds. The digital nature of $\bar{n}$ is a drawback in a chemical coordinate. The overall correlation is rather poor.

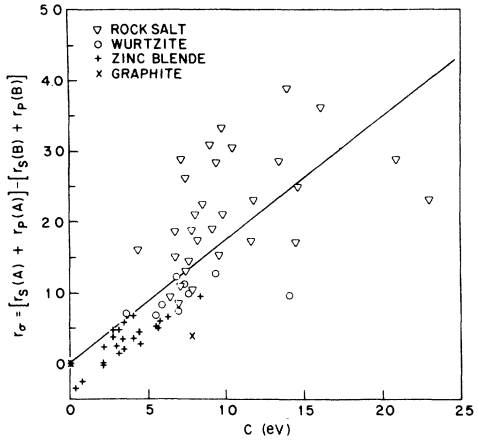

FIG. 7. St. John–Bloch coordinate r_σ vs the Phillips–Van Vechten ionicity parameter C for 67 octet binary compounds. The reader may note that the linear correlation is better for small values of C than for large ones, that is, it is poor for rocksalt compounds. This reflects the classical closed-shell character of the latter, which is not described well by either coordinate.

from $\bar{n}=1$ to $\bar{n}=5$ in the group-IV column is a good example.) With respect to r_π we note it measures an average of the s-p splittings of the atoms. Thus r_π increases, for example, from C to Pb and should correlate to some extent as $\bar{n}$. In Fig. 6 we see that there exists no strong correlation. However, the structures do tend to cluster in rows, particularly near $r_\pi \approx 1-2$ (which correspond to alkali halide series, e.g., LiF, LiCl, LiBr, LiI, etc.) and the rows do tend toward a positive slope. Another observation is that for any given $\bar{n}$ there exists a trend with increasing values of r_π to go from a covalent to ionic structure. For example, with $\bar{n}=1$ with increasing r_π there exist graphite, wurtzite, and rocksalt structures, respectively, and for any $\bar{n}$ the largest r_π value corresponds to a rocksalt crystal.

In summary, with respect to the MP coordinates, while ΔX correlates fairly well with r_σ, r_π does not correlate with $\bar{n}$. In particular, the digitalized form of $\bar{n}$ appears to represent a serious drawback to its use as a chemical coordinate.

In Fig. 7 we plot the dielectric coordinate C against the bond orbital coordinate r_σ. C is an ionicity parameter defined such that it measures the ionic contribution to the average gap between bonding and antibonding states in tetrahedrally coordinated binaries. Overall, the correlation is not so good as the Pauling ΔX-vs-r_σ plot. For the more-ionic rocksalt compounds in particular, there is a wide scatter of the points. This may result from a failure of the PVV ionicity parameter to describe accurately large deviations from the covalent case, or simply the breakdown of linear scales in the strong-interaction closed-shell ionic limit. The correlation between ΔX and r_σ may be superior to the correlation between C and r_σ because ΔX and r_σ are derived from atomic properties; however, C is restricted in its meaning to tetrahedrally bonded crystals. We note that C by itself fails in the same region as ΔX to distinguish between wurtzite and rocksalt structures. Finally, in Fig. 7 we find the best linear fit to the data comes from

$$r_\sigma = 0.174C + 0.023 \ , \tag{12}$$

where C is in eV and r_σ in a.u. It is interesting to note that the constant in (12) is very small, compared, e.g., to the constant in (11).

For the last comparison we have plotted r_π versus the dielectric coordinate E_h. E_h represents a covalent, or homopolar, contribution to the energy gap. Van Vechten found that for group-IV materials $E_h \sim d^{-2.5}$, where d is the bond length. If we do a similar analysis for r_π we find $r_\pi \sim d^{2.5}$ implying that $E_h \sim r_\pi^{-1}$. In fact a log-log plot for E_h vs r_π was made and a least-squares fit to the result yielded $E_h \sim r_\pi^{-0.92}$. In Fig. 8 we display the results for r_π vs E_h^{-1}. The best fit displayed in Fig. 8 is given by

$$r_\pi = 2.64/E_h + 0.14 \ , \tag{13}$$

where E_h is given in eV and r_π in a.u. Overall, the agreement is fairly good, certainly better than an r_π-vs-$\bar{n}$ plot. As expected those compounds with the largest E_h correspond to the covalent graphite

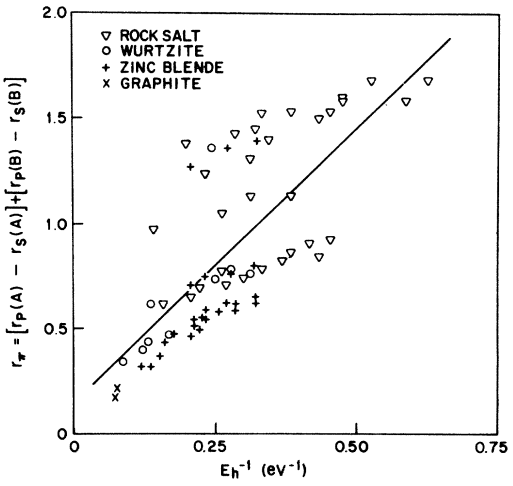

FIG. 8. St. John–Bloch coordinate r_π vs the inverse of the Phillips–Van Vechten covalent energy gap E_h for 67 octet binary compounds. r_π measures, in part, the degree of metallization present in the binary and thus correlates with E_h^{-1}.

structure C and BN. However, this plot fails to make any strong correlation with structure.

In summary, we find that trends do exist between (r_σ, r_π) and (C, E_h^{-1}) or $(\Delta X, \bar{n})$; in some cases they are qualitative at best. Of course, this is obviously not a bad result; if an exact correlation were found there would be no advantage in the (r_σ, r_π) coordinates over the (C, E_h) or $(\Delta X, \bar{n})$ coordinates.

IV. APPLICATION OF THE BLOCH-SIMONS RADII TO THE STRUCTURAL STABILITY OF BINARY COMPOUNDS

In a recent publication, St. John and Bloch[10] applied their coordinate scheme to 63 binary compounds $A^N B^{8-N}$. In this section we extend their results to include the noble metals Cu, Ag, and Au. These metals have been a source of trouble in the construction of classical electronegativity scales. Chemically they may exhibit a valence of either $Z = 1$ or $Z = 2$; the reason being that the promotion energy from $d^{10}s^1$ to d^9s^2 is quite small.[24]

In Fig. 9 we display the results for 79 binary octet crystals. In addition to the usual compounds as tabulated by Van Vechten[24] we have included the noble metal compounds as labeled in the figure, some barium and mercury chalcogenides, and some cesium chloride structures. We have handled the dimorphous compounds in a similar manner to the St. John–Bloch plots. We consider only the most stable compounds at zero temperature and pressure. In the case of the fourfold coordinated compounds we place those which form polytypes into the zinc-blende class. This classification is based upon the thermodynamic arguments of Jagodzinski.[10,25] MgS and MgSe, which border the zinc-blende–wurtzite separation, are classified as rock salts. These compounds will condense from the gas phase into wurtzite structures and then slowly undergo a phase transformation into a stable rocksalt structure.[26,27]

The general topology of the bond-orbital plot the graphite structures C and BN at one end and the eightfold coordinated compounds of the CsCl structure at the other extreme. Going from C to CsCl along a line we traverse from threefold, fourfold, sixfold to eightfold coordination. The great success of the bond-orbital plot as opposed to the dielectric separation scheme lies in its capacity of distinguishing between the wurtzite and zinc-blende structures. This very delicate separation depends on changes in the position of third nearest neighbors.[10]

We shall now examine the Cu and Ag halide groups. As a class they fall below the main body of the binaries. Nevertheless, the separation of rock salt from zinc-blende structure remains. One noticeable failure, however, is the case of CuF. It appears to fall into the rocksalt group, yet presumably it has a zinc-blende structure according to Wyckoff.[28] This classification is from the 1933 work of Ebert and Woitneck.[29]

We note that the SB plot does not indicate the existence or nonexistence of compounds; nor whether the AB binary might be more stable than, for example, AB_2. In the example at hand, CuF probably does not exist at all. Barber, Linett, and Taylor[30]

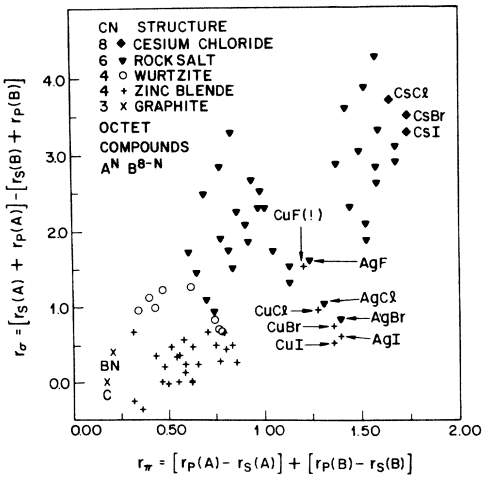

FIG. 9. St. John–Bloch plot for 79 binary octet crystals $A^N B^{8-N}$. Note in particular the separation of the wurtzite from the zinc-blende structures. This separation was not possible with the dielectric method. CuF, although tabulated by Wyckoff (Ref. 28) as a zinc-blende binary, does not exist as a stable compound (see text).

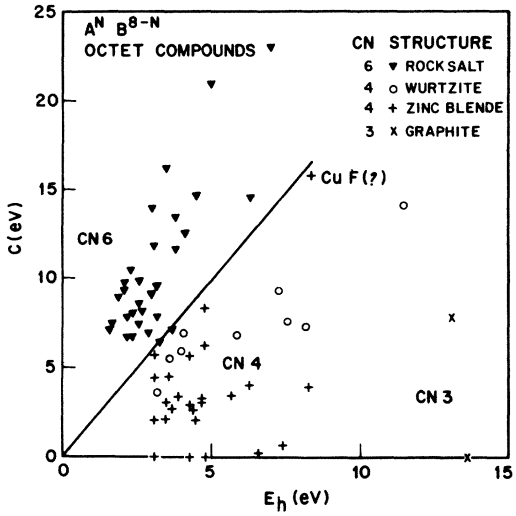

FIG. 10. Phillips–Van Vechten diagram for octet binary compounds. The (C, E_h) coordinates result in the exact separation of fourfold and sixfold coordinated compounds, but do not separate the zinc blendes from the wurtzites as do the St. John–Bloch coordinates. For a discussion of the special case of CuF see the text. The coordination number (CN) is listed for each crystal structure.

have noted that although CuF has been reported in the literature, its existence is now in doubt. In particular, the method by which Ebert and Woitneck prepared CuF has been questioned by Wartenburg.[31] It is now thought that CuF might exist only

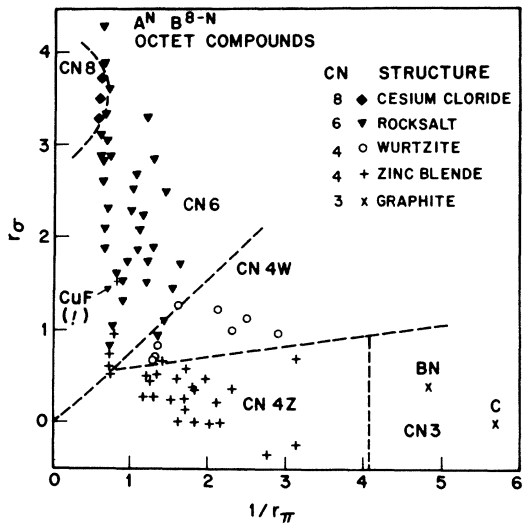

FIG. 11. Bond-orbital separation for 79 binary octet compounds using the coordinates (r_σ, r_π^{-1}). Note the resemblance to the Phillips–Van Vechten plot (Fig. 10). The special case of CuF is discussed in the text. The coordination number (CN) is listed for each crystal structure.

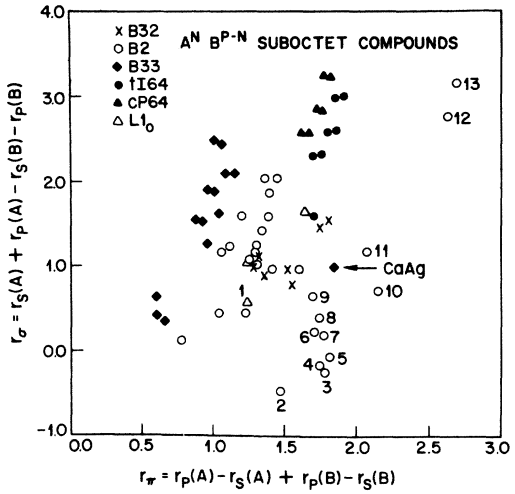

FIG. 12. St. John–Bloch diagram for the suboctet binary compounds $A^N B^{P-N}$ $(2<P<6)$. For a list of the compounds except for the (Cu, Ag, Au) binaries see Ref. 15. The numbered compounds correspond to AuCl (1), BeCu (2), ZnCu (3), ZnAg (4), CdAg (5), MgAu (9), LiAg (10), LiAu (11), RbAu (12), and CsAu (13). The special case of CaAg is discussed in the text.

in admixtures of CuF_2.[30,31] This example nicely illustrates the power of our plots. Because of the discrepancy occurring in Fig. 9 (between predicted and observed structures), an examination of the literature was performed with the consequent discovery of the nonexistence of CuF. This discrepancy does not occur in the Mooser-Pearson diagrams[1] or the Phillips–Van Vechten diagram[6] (Fig. 10). According to Eqs. (12) and (13), the bond-orbital separation will resemble the dielectric one if we use (r_π^{-1}, r_σ) as coordinates corresponding to (E_h, C). This is shown in Fig. 11, and the similarity to Fig. 10 is evident.

In Fig. 12 we display a similar plot for binary compounds which belong to the suboctet group $A^N B^{P-N}$. We have extended the results of Machlin, Chow, and Phillips[15] to 67 binaries including the noble-metal compounds. The binaries considered correspond to two broad classes: 40 structures which are derived from bcc CsCl structures and 27 anion valence coordination structures. In Fig. 12 the bcc structures are represented by open symbols, the anion coordinated structures by solid symbols. The former structural types correspond to the crystal classes $B2$ $(cP2)$, $L1_0$ $(tP4)$, and $B32$ $(cF16)$. The latter group of anion valence coordinated compounds form anion zigzag chain structures, cf. Se and Te such as the $B33$ $(oC8)$ structures, with $P - 2N = 2$ anion-anion bonds per anion and anion tetrahedral clusters (perfect $tI64$ and imperfect $cP64$) with $P - 2N = 3$. Both $tI64$ $(tP4)$ and $cP64$ can be considered as distorted boundary

phases, just as wurtzite is a distorted boundary phase for octet compounds. The interested reader is referred to Pearson for a more-detailed discussion.[32]

Figure 12 shows that the bond-orbital coordinates separate not only the two broad classes of structures, but for the most part, the six separate crystal structures as well. There is an area of confusion, however, in the $r_\pi \approx 1.7$, $r_\sigma \approx 1.5$ region. It has been suggested that a successful separation can be achieved in this region by using the normalized coordinates: $r_i^\alpha / r_{12}^\alpha$, where r_{12} is the standard close-packed atomic radius.[15]

Before discussing the noble metal additions, we shall review the general conclusions presented elsewhere.[15] The most significant information presented in Fig. 12 is that the *same* coordinates which separated $A^N B^{8-N}$ separate $A^N B^{P-N}$ where $P \approx 4$. This suggests that these coordinates are the proper coordinates for almost all nontransition metal structures for a wide range of P. Exceptions for these coordinates may occur for small values of P (~2) where exchange and correlation are especially important. In such cases the energy differences between the various structures can typically be of the order of correlation energy differences.

The noble-metal compounds are labeled in Fig. 12 by number, with the exception of CaAg which is explicitly labeled. The addition of these compounds does not alter the general separation scheme with the exception of CaAg. CaAg belongs to the $B33$ structure which has as prototypes of this structure CrB,[33,34] and TlI.[35] (Other members in this family include, e.g., CaSi, SrGe, BaPb, and InBr.) We include the halides in this group for comparison although properly they are "super" octets with $P \approx 10$. Although CaAg has the $B33$ structure, on the basis of its other properties it appears to hold a unique position. This is illustrated in Table II where we have detailed the cation-cation, cation-anion, and anion-anion distances, the ratio of the cation-anion distance to the anion-anion distance, the anion-anion angle for the anion chains and the electronegativity differences of SB and Pauling. We note the existence of strong correlations between the electronegativity differences of the orbital shell model, Eq. (5), with both the cation-anion–to–anion-anion ratios and the anion chain angle. For the reader's convenience the anion chain angle is illustrated[33] in Fig. 13 for CaSi.

In conventional chemical bond theory the formation of the $B33$ structure in simple metallic compounds is explained by the fact that with $P - 2N = 2$ there are two electrons/anion free to form anion-anion bonds which are required for anion-anion chains. However, this qualitative explanation does not account quantitatively for trends in internal structural parameters. Presumably this is one of the reasons why Parthe has said[35] that "Simple ideas on crystal structure formation using size effects, number of valence electrons, etc., are just not sufficient" for the $B33$ and related structures.

We have plotted in Fig. 14 the anion-anion bond angles θ for these compounds. The angles span a wide range from 95° to almost 110°. The figure dramatizes the fact that θ is a linear function of $\Delta\tilde{X} = \tilde{X}(A) - \tilde{X}(B)$ to within better than 1°, where $\tilde{X}$

TABLE II. Structural parameters for the CrB ($B33$) structures. $d_{c\text{-}c}$, $d_{c\text{-}a}$, and $d_{a\text{-}a}$ are the nearest-neighbor distances for the cation-cation, cation-anion, and anion-anion, respectively. θ_{aa} is the anion-anion angle for the anion chains (see Fig. 13). The parameters were obtained from Refs. 33–35. Electronegativity differences from St. John–Bloch and Pauling (see Table I) are also tabulated.

Compound	$d_{c\text{-}c}$	$d_{a\text{-}a}$	$d_{c\text{-}a}$	θ_{aa}	$(d_{c\text{-}a}/d_{a\text{-}a})^{-1}$	$\Delta X_{\text{St. John–Bloch}}$	$\Delta X_{\text{Pauling}}$
CaSn	3.79	2.90	3.27	96.6	0.128	0.33	0.9
CaAg	3.66	2.89	2.99	106.9	0.0346	0.41	0.9
SrSn	3.88	2.93	3.43	100.4	0.171	0.42	0.8
BaSn	4.03	2.97	3.60	102.2	0.205	0.48	0.9
BaPb	3.79	2.90	3.61	99.7	0.245	0.49	0.8
CaGe	3.56	2.59	3.12	100.7	0.205	0.52	0.8
CaSi	3.59	2.47	3.11	104.6	0.259	0.57	0.8
SrGe	3.77	2.62	3.27	105.3	0.248	0.61	0.8
SrSi	3.76	2.51	3.26	106.6	0.299	0.66	0.8
BaGe	3.97	2.64	3.44	109.2	0.303	0.67	0.9
BaSi	3.93	2.54	3.38	108.8	0.331	0.72	0.9
TlI	3.83	4.33	3.34	74.8	−0.115	0.30	0.7
InI	3.58	4.34	3.23	67.1	−0.266	0.35	0.8
InBr	3.68	3.94	2.80	61.6	−0.289	0.61	1.1

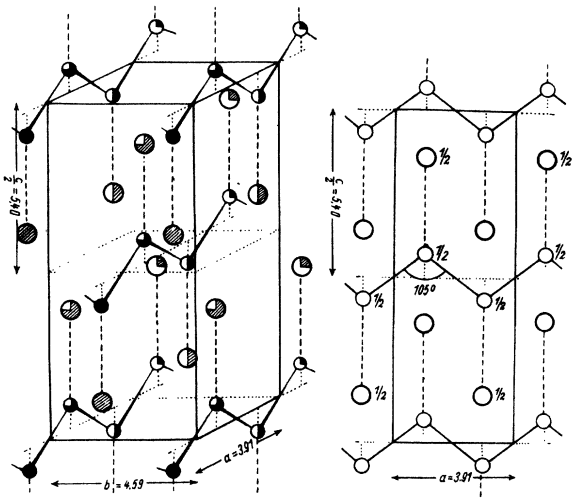

FIG. 13. CrB ($B33$) structure. The anion-anion chains are shown with the value of $\theta_{aa}=105°$ appropriate to CaSi. The figure is taken from the work of Kiessling (Ref. 33).

is given by Eq. (5). We consider this to be remarkable correlation, which, as Parthe remarks, cannot be achieved with classical (orbitally independent) coordinates.

The fact that CaAg does not group with the other $B33$'s is indicative of its special nature. Unlike the others, CaAg has catalytic properties. The Ag-Ca

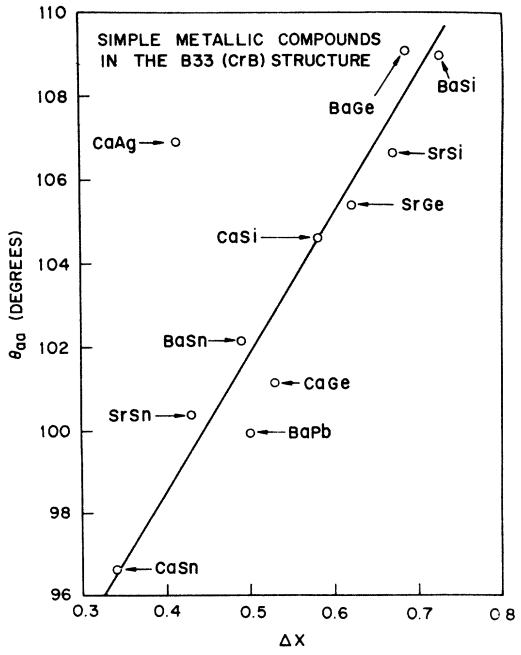

FIG. 14. Anion-anion chain angle θ_{aa} displayed as a function of the St. John–Bloch electronegativity ΔX. Note the anomalous behavior of CaAg.

alloy, known as Raney Ag, is used as a catalyst in oxidation-reduction reactions such as the conversion of ethylene to ethylene oxide.[36] In fact, its exceptional position in the SB plot suggested that CaAg might have unusual properties. This emphasizes the usefulness of such plots.

Another example of a significant correlation between structure and properties occurs in the cases of CsAu and RbAu (labeled 12 and 13 in Fig. 12). These crystals are separated by a large distance in the SB plot from the other $B2$ crystals suggesting again some special properties associated with them. In fact, CsAu and RbAu are semiconductors unlike the other $B2$'s.[37-39] CsAu is thought to be a semiconductor with a band gap of approximately 2.5 eV. It also displays some rather interesting optical absorption structure in this region which is thought to be excitonic in nature. On the basis of band calculations for the alkali series LiAu, NaAu, KAu, RbAu, and CsAu, Huang and Liu have hypothesized that a metal-semiconductor transition takes place between KAu and RbAu.[37] This is in agreement with previous speculations on the character of NaAu and KAu.[39] Unfortunately, little work has been done on NaAu and KAu, and at present it is not clear to what crystal structure they correspond. Thus they have not been included on Fig. 12, but they would fall in the gap between LiAu and RbAu (compounds 11 and 12).

Finally, with respect to the suboctet structures, we note the placement of the "superoctet" $B33$'s ($r_\pi = r_\sigma \approx 0.5$). While these $P=10$ binaries also have the CrB structure, the internal parameters as listed in Table II indicates that the bonding properties in these compounds are quite different from the suboctet group. For example, the ratio of cation-anion–to–anion-anion distances is less than unity, and the anion chains have ceased to be important. If we define an anion-anion angle as for the suboctet group we see the angle changes systematically with ionicity (as defined by Pauling or St. John and Bloch). Likewise, the distance ratios also correlate well; however, both the distances and the angles correlate *inversely* with ionicity differences in contrast to the suboctet compounds.

We now turn to the prediction of melting points T_f for the suboctet compounds. The theory of melting points, as in the case of crystal structures, involves small energy and entropy differences and is thus a particularly difficult subject. With the exception of Van Vechten's[40] recent work on $A^N B^{8-N}$ semiconductors, no major advance on the theory of T_f has occurred since the work of Lindemann[41] in 1910. The reader will recall that Lindemann proposed that a crystal should melt when the mean amplitude of the thermal vibration $\bar{x}$ of one of its constituent atomic species reached

a critical value x_c. Thus, Lindemann proposed the following expression for T_f:

$$T_f = x_c^2 M \Theta_D^2 / 8\hbar^2 , \tag{14}$$

where M is the atomic mass and Θ_D is the Debye temperature. Typically x_c is one-quarter of the atomic radius.[42] While (14) is a useful expression for estimating T_f, as Van Vechten[40] notes it is of limited practical use for estimating T_f as it reqires a knowledge of Θ_D. Since Θ_D is usually more difficult to obtain than T_f, it is common to invert (11) and use the observed value of T_f to estimate Θ_D.

Van Vechten's analysis of the melting points of semiconductors is based on scaling the bond energies occurring in the dielectric theory of the octet semiconductors. Given certain experimental data on Si, i.e., the heat and entropy of fusion, the Debye temperature, and the pressure at which Si transforms into the β-tin structure, Van Vechten was able to predict the melting temperatures of most IV-IV, III-V, and II-VI semiconductors within an accuracy of 10%. While this approach is superior to Lindemann's treatment in that it does not require a knowledge of Θ_D (except for Si), it unfortunately is applicable only to the binaries for which the dielectric theory can be used. In addition, Van Vechten's results are based on the assumption of a liquid phase which is metallic. Therefore, it cannot be applied to crystals which melt into an insulating liquid such as CuCl. Finally, problems also arise in cases such as the arsenide binaries, e.g., GaAs, where the As tends to associate in the liquid.

In the present context we consider the melting temperatures of some 40 suboctet compounds. One advantage of studying the suboctet groups is that the problem associated with liquid-anion association in octet binaries is reduced in the case of the suboctets as the constituents are largely cationic. The basis of our treatment of melting points resides in the accuracy of the structural separation achieved with the bond-orbital coordinates (r_σ, r_π). Since these coordinates appear to be very accurate chemical coordinates, we expect them to be able to distinguish between the various melting points. To examine this possibilty we assume that the melting temperatures may be expressed as function of (r_σ, r_π). Thus, we take

$$T_f = T_f(r_\sigma, r_\pi) \tag{15}$$

and expand T_f to second order:

$$T_f(r_\sigma, r_\pi) = a_0 + a_1 r_\sigma + a_2 r_\pi + a_3 r_\sigma r_\pi + a_4 r_\sigma^2 + a_5 r_\pi^2 \tag{16}$$

In a similar fashion we may attempt to understand the melting temperature point behavior by an expansion in the simple-model (Mooser-Pearson) coordinates $(\bar{n}, \Delta X)$:

$$T_f(\bar{n}, \Delta X) = b_0 + b_1 \Delta X + b_2 \bar{n} + b_3 \bar{n} \Delta X + b_4 \Delta X^2 + b_5 \bar{n}^2 . \tag{17}$$

The expansion coefficients in both cases were detemined by a fit to the experimental melting points. In the fitting procedure we excluded from consideration the suboctet compounds which undergo structural transformations before melting. Another problem with the experimental data is the lack of information on the $tI64$ and $cP64$ structures. These structures include such compounds as KGe, NaPb, and RbSi. Members of this family tend to sublimate. However, of the remaining structures melting temperatures are available for the majority of cases.[43]

The resulting coefficients for Eqs. (16) and (17) are presented in Table III. In Table IV the predicted melting points on the basis of (16) and (17) are compared to the experimentally determined melting temperatures. We have also plotted the results listed in Table IV in Figs. 15 and 16.

Overall the orbital shell-model results displayed in Fig. 15 are in reasonably good accord with experiment. The rms error, neglecting the anomalous behavior of MgAu which will be discussed below, is less than 140 °K; the predictive accuracy of (16) is therefore on the order of 15%. In the case of the simple shell model the attempt to fit (17) to experiment results in the very poor fit exhibited in Fig. 16. The rms error is over 260 °K and the average deviation is almost 30%. The major problem of the Mooser-Pearson simple shell-model coordinates is their inability to distinguish between compounds on the basis of $\bar{n}$ and ΔX alone. For example, consider the compounds SrSi and LiTl. Both suboctets have $\bar{n} = 3$ and $\Delta X = 0.8$ and as a consequence the Mooser-Pearson expression assigns

TABLE III. Expansion coefficients [Eqs. (16) and (17)] for the melting points of suboctet compounds. The units are such that if (r_σ, r_π) are in atomic units or ΔX is from Table I, then T_f is in °K.

	Bloch-Simons		Mooser-Pearson
a_0	1410	b_0	570
a_1	−1400	b_1	2080
a_2	940	b_2	−345
a_3	−640	b_3	110
a_4	660	b_4	−1220
a_5	54	b_5	35

TABLE IV. Predicted and observed melting points for the suboctet compounds $A^N B^{P-N}$. The experimental data are from Ref. 43. Experimental values in parentheses were not used to fit the expansion coefficients [Eqs. (16) and (17)] as these compounds undergo structural transitions before they melt. Note the anomalous behavior of MgAu.

Compound	Melting points (°K) Experimental (°K)	Predicted Bloch-Simons	Mooser-Pearson
CaAg	938	906	1030
BaPb	1123	1330	1109
BaGe	1418	1570	1039
CaGe	1573	1344	1003
CaSi	1518	1405	1035
CaSn	1260	1178	989
SrSi	1423	1486	1003
SrGe	1438	1420	989
TlI	723	966	936
CdAg	(1003)	1079	203
LiAu	(1159)	1191	1064
MgAg	1093	987	944
ZnAg	(963)	1083	420
CdAu	900	930	936
LiAu	918	986	849
MgAu	1423[a]	879	673
RbAu	773	670	748
ZnAu	998	931	992
BeCu	(1203)	809	745
CaCd	(958)	903	924
CaTl	1243	923	1038
CaHg	1234	1033	992
SrCd	973	948	921
ZnCu	(1153)	1029	462
LiHg	868	839	1038
MgHg	900	773	924
LiPb	755	872	1003
LiTl	783	841	1003
MgTl	628	805	834
LiAl	991	876	949
LiCd	822	828	980
LiGa	999	892	963
LiIn	910	839	980
NaIn	713	842	1003
LiZn	753	833	963
NaTl	578	839	1030
LiBi	878	909	1038
NaBi	793	860	1046
NaPb	641	844	1030
KPb	843	853	1061
KSn	1103	885	1046
BaCd	854	1024	1005
BaHg	1095	1025	1130
HgSr	1133	964	1055

[a] See text.

them identical melting temperatures of 1003 °K; however, experimentally SrSi melts at 1423 °K and LiTl at 783 °K. The orbital shell-model coordinates yield predicted melting points of 1486 °K for SrSi and 841 °K for LiTl in good agreement with experiment. These results illustrate the superiority of the latter coordinates over those of the Mooser-Pearson simple shell model.

With respect to the structural plots for the suboctet compounds in Fig. 12, several interesting observations can be made. The low-melting-temperature compounds lie on a line which roughly passes through CaAg and RbAu. With compounds which lie some distance in a direction perpendicular to this line, the melting temperatures increase fairly rapidly. For example, the CrB com-

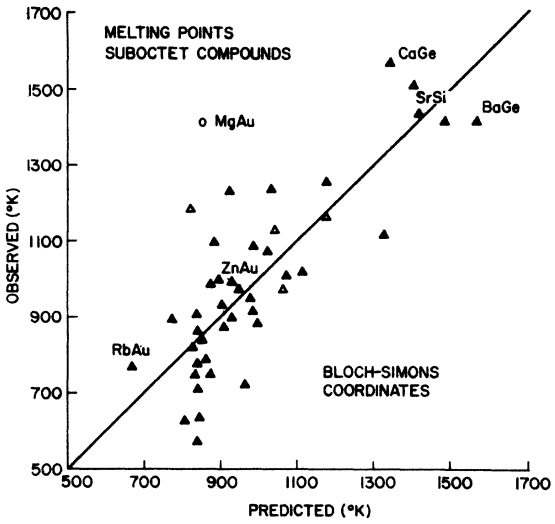

FIG. 15. Observed and predicted melting points for 44 suboctet binary compounds. The predicted melting points are from Eq. (16) which is based on the Bloch-Simons Coordinates. The open symbols were not used to determine the expansion parameters. The anomalous behavior of MgAu is discussed in the text.

pounds such as SrSi or BaGe have a very high melting point compared to compounds such as NaTl or LiPb which lie near the CaAg-RbAu line. The CrB compounds have rather large values of r_σ and small values of r_π. In analogy to the Phillips–Van

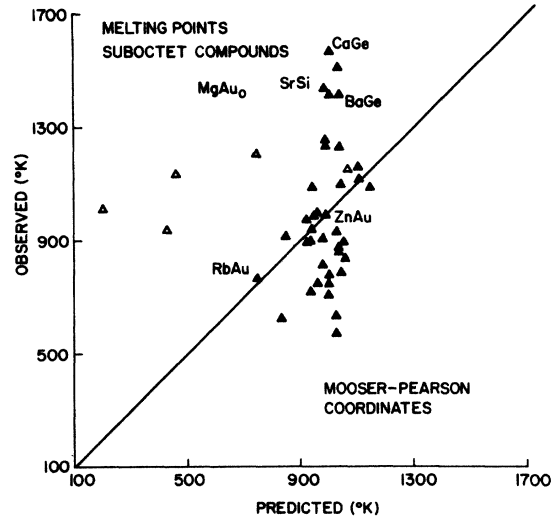

FIG. 16. Observed and predicted melting points for 44 suboctet binary compounds. The predicted melting points are from Eq. (17) which is based upon the Mooser-Pearson coordinates. The rather poor predictive powers of the Mooser-Pearson coordinates is indicated by the poor correlation. The open symbols were not used to determine the expansion parameters. The anomalous behavior of MgAu is discussed in the text.

Vechten coordinates, this implies large values of C and E_h, respectively. Therefore, perhaps it is not too surprising that such structures have high melting temperatures.

A similar examination of a Mooser-Pearson plot in an attempt to understand the melting points would be difficult on the basis of the fit in (17). The fit is so poor that the addition or deletion of just a few compounds can radically change the values of the expansion coefficients. Therefore, it is risky to interpret the coefficients in physical terms. About the only observation which can be made is that the index $\bar{n}$ appears to play a minor role which again occurs because of its digitalized form.

With respect to Fig. 15 we note the anomalously high melting point of MgAu. From Table IV we obtain the predicted melting point of MgAu to be 879 °K. The difference is almost four standard deviations away from the fit to the remaining compounds. In addition, the behavior of similar valence compounds such as ZnAu and CdAu appear to be correctly described, thus adding to the bizarre behavior exhibited by MgAu. Pearson[44] has discussed the anomalous behavior of MgAu in terms of electronegativity differences as the atomic radii of Mg and Cd are nearly identical. On Pauling's scale $\Delta X(\mathrm{MgAu}) = 1.2$, while $\Delta X(\mathrm{CdAu}) = 0.7$. Thus Pearson proposes to account for the 520 °K difference in melting points between CdAu and MgAu as a charge transfer effect. However, on the basis of the St. John–Bloch scale we would find $\Delta X(\mathrm{MgAu}) = 1.1$ and $\Delta X(\mathrm{CdAu}) = 1.0$ which would not account for such a large melting point difference. We prefer to attribute the anomaly to the character of Au as nearly a transition metal element, which means that r_d plays an important role. Further discussion of this point is given in Appendix A.

Finally, with respect to Fig. 15 we observe that several suboctet compounds on the basis of the orbital shell-model coordinates are predicted to have higher melting points than observed. These compounds cluster in the lower left-hand corner of Fig. 15 and include, e.g., NaPb, NaTl, MgTl, and LiPb. Their presence results in the sharp turn down of the experimental melting points compared to the theoretical values near 850 °K in Fig. 15. It is interesting to speculate that the behavior of these compounds may be analogous to that observed in the octet semiconductors. In this case, it has been found that for large values of the Phillips ionicity parameter the semiconductor lattice tends to soften as the ionicity nears a critical value separating the tetrahedral configuration from the more ionic sixfold coordinated rocksalt structure.[45,46] If a similar softening occurs for the suboctet compounds this might be reflected in the re-

duced melting temperature and deviations occurring from the predicted melting points. Such a softening, possibly of a zone-boundary acoustical phonon, could be detected in several ways, e.g., in specific-heat data. According to Table IV, the greatest softening probably occurs in NaTl, where $T_{f\,(\text{expt})}$ is 250 °C below $T_{f\,(\text{theor})}$.

V. UNIAXIAL STRAINS

In this section we discuss uniaxial strains in two families of tetrahedrally coordinated octet semiconductors, the wurtzite simple binary family and the chalcopyrite pseudobinary family. These strains are known very accurately. We hope that chemical trends in these strains can be correlated with bond-orbital coordinates.

The stability of octet wurtzite compounds has been discussed carefully by Lawaetz.[47] He has shown that there is a close empirical correlation between c/a and the stability of wurtzite-versus-sphalerite (hexagonal-versus-cubic) modifications. He concludes that the critical parameter Δ given by

$$\Delta = c/a - 1.633 \tag{18}$$

must be negative (within at least 0.1%) for the wurtzite modification to be stable. Moreover, the range of c/a values for which the materials are dimorphous extends about equally to both sides of the ideal value $\Delta = 0$. This suggests that the relationship between the energy difference and Δ is almost linear.

Lawaetz further identifies this energy difference with $y = (ZC/\hbar\omega_p)^2$ and shows that there is a good linear correlation between y and Δ. The parameter y involves Z, the formal cationic charge (or the number of Pauling resonating bonds), the Phillips ionic energy gap C, and the plasma energy $\hbar\omega_p$. This rather unexpected combination of parameters also correlates well with the Szigetti effective dynamical charge e_s^* for lattice vibrations.[48]

From Fig. 9 we see that on a bond-orbital or SB plot the boundary between sphalerite and wurtzite structures is perpendicular to the r_σ coordinate. This suggests that we examine the correlation between $y' = r_\sigma/a$ and Δ. (Both y and y' are normalized dimensionless coordinates. Here a is the wurtzite lattice constant in the basal plane.) This correlation is shown in Fig. 17. It should be compared with Fig. 3 of Lawaetz.[47] The two are remarkably similar; the worst fits in both cases include BN and BeO.

We have found in general that our structural plots are more satisfactory if we use non-normalized coordinates. (This implies that it is the shell structure of the ion cores and not the atomic cell

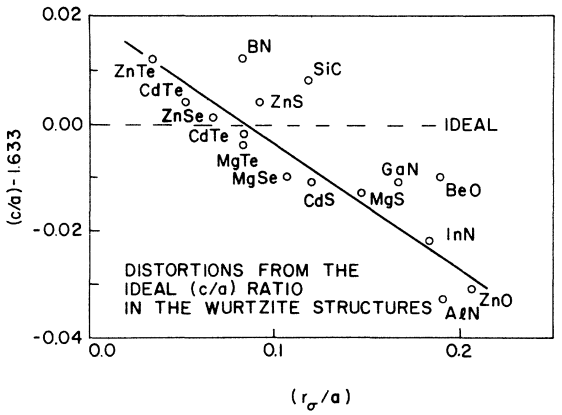

FIG. 17. Distortions of the c/a ratio from the ideal value for several wurtzite binaries as a function of the normalized Bloch-Simon coordinate r_σ/a. The results are quite similar to those obtained by Lawaetz (Ref. 47).

dimensions or outer atomic wave functions which are of primary structural significance; therefore, it is not correct to normalize the former by the latter.) In Fig. 18 we show the non-normalized plot of Δ against r_σ. Comparing Fig. 18 with Fig. 17, we argue that r_σ is a better configuration coordinate than r_σ/a. Note that in Fig. 18 three compounds, BN, SiC, and BeO have moved much closer to the line. Two compounds AlN and ZnO, have moved away, but these are the compounds for which $|\Delta|$ is the largest, and for which a nonlinear increase in $|\Delta|$ with r_σ (similar to what is shown in Fig. 19 for the chalcopyrite distortions) might be expected.

We next investigate the structural trends in the ternary tetrahedral compounds: the $A^{II}B^{IV}C_2^V$ chalcopyrites.[49-52] Just as the binary compounds

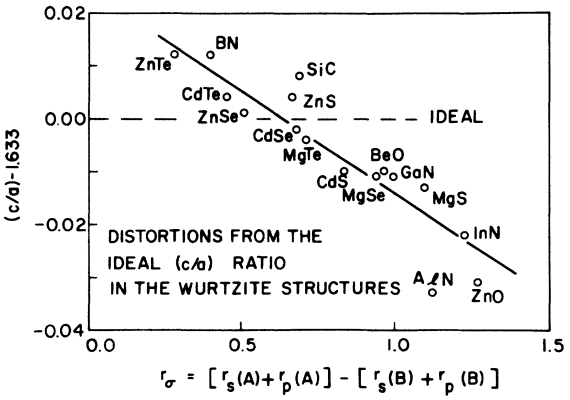

FIG. 18. Distortions of the c/a ratio from the ideal value for several wurtzite binaries as a function of the nonnormalized Bloch-Simons coordinate r_σ. Note the improvement over the results obtained with r_σ/a as in Fig. 17.

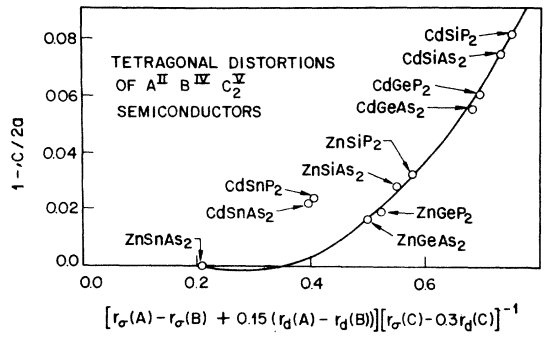

FIG. 19. Tetragonal strain for $A^{II}B^{IV}C_2^V$ chalcopyrite semiconductors plotted as a function of a suitable combination of bond orbital coordinates.

A^NB^{8-N} are analogous to diamondlike crystals A^{IV}, so these ternary compounds are analogous to the binary ones. The primary difference is that the ternaries contain two types of cations. In the chalcopyrite structure each A-type of cation has as a second nearest neighbor 8 B cations and 4 A cations. These are distributed with 4 B cations in the x-y plane, and 2 A and 2 B cations in the x-y and y-z planes. A key feature of this arrangement is the presence of A-C-A and B-C-B linkages parallel to the x axis. This difference in linkages causes a tetragonal contraction along the z axis, which contains only A-C-B linkages. This results in $c/2a$ being less than unity by typically 0.05. Thus it appears that chalcopyrite compounds are stable only for $c/a-2<0$, just as wurtzite compounds were stable only for $\Delta<0$. Crystallographic studies of trends in $c/2a$ among chalcopyrites using combinations of atomic radii have been only qualitatively successful.[50] This is not a surprising result; for covalent crystals polarization effects may dominate thus invalidating this sort of "rigid-ion" approach.

Another approach has been to describe the charge redistribution taking place in terms of elemental electronegativities. In such an approach it becomes apparent that Pauling's electronegativity scale is not appropriate. For example, $1-c/2a$ varies from 0.081 for $CdSiP_2$ to 0.025 for $CdSnP_2$ but Pauling lumps Si, Ge, and Sn together with the same electronegativity of 1.8. Therefore, Phillips used an electronegativity scale based upon the dielectric method in an attempt to understand the tetragonal distortions.[50] He was able to obtain a reasonable fit to the experimental values by taking

$$2-c/a=-0.6X_A+0.25X_B+0.15X_C+0.01. \quad (19)$$

This linearized expression yields accurate results for small distortions, but it underestimates the observed values for large distributions. Phillips was also able to note the coefficient in (19) suggested a contribution to the distortion which depended three times more on the charge transfer involved with atom A as compared to atoms B or C. In fact, he observed the coefficients in (19) scale roughly as $1/Z_\alpha$.

TABLE V. Average cation spin-orbit splitting for several $A^{II}B^{IV}C_2^V$ chalcopyrites, $\Delta_{SO}(AB)=\frac{1}{2}[\Delta(A)+\Delta(B)]$, compared to the crystal-field splittings, Δ_{cf}. The experimental values are taken from Ref. 52. Note the very large value for Δ_{SO} compared to Δ_{cf} for the case of $CdSnAs_2$. The energies are in eV.

Compound	$\Delta_{SO}(AB)$	Δ_{cf}	$\Delta_{SO}(AB)/\Delta_{cf}$
$CdSiAs_2$	0.14	0.24	0.6
$CdGeP_2$	0.26	0.20	1.3
$ZnSiP_2$	0.06	0.13	0.5
$ZnGeP_2$	0.18	0.08	2.2
$CdSnAs_2$	0.47	0.06	7.8

We have attempted to undertake a similar study with the Bloch-Simons radii as the basis of correlating the distortions. Unlike the previous approaches using atomic radii, the Bloch-Simons radii are orbitally dependent and thus should provide a basis for the chemical trends resulting in the tetragonal distortions. As a first attempt to find a relationship between $c/2a$ and the radii, we considered the quantity $r_\sigma=r_\sigma(A)-r_\sigma(B)$ in a similar fashion to the structural plots. However, this approach is only qualitatively successful. The major defect of this coordinate is that it does not distinguish between the anions. Also since the d radii appear nowhere in r_σ the coordinate cannot distinguish between Si and Ge chalcopyrites.

A number of alternate coordinates were considered before we found the correlation presented in Fig. 19. In order to distinguish between Ge and Si we have included an $r_d(A)-r_d(B)$ correction, and further to distinguish among cations we include an $r_\sigma(C)$ term. The denominator correction is small being on the order of 10%. Unfortunately two notable exceptions to the smooth curve in Fig. 19 occur: $CdSnP_2$ and $CdSnAs_2$. This result can be attributed to the presence of a very large spin-orbit splitting on the cations. For the reader's convenience the cation spin-orbit splittings are compared[52] to the crystal-field splittings for several compounds in Table V.

VI. GLOBAL THERMOCHEMICAL MODEL

The binary phase diagrams of more than 500 metallic alloys have been investigated extensively by many workers over a long period.[2] In a few cases the diagrams are rather simple, corresponding perhaps to nearly ideal liquid and regular solid solutions. In most cases, however, the dia-

grams are quite complex, because there are a number of competing solid phases which are either alloys or compounds. Theoretical analysis of these diagrams has become correspondingly sophisticated as evidenced by the pioneering work of Kaufmann.[53] The current state of the art is reflected in the specialist papers in the new journal Computer Analysis of Phase Diagrams and Thermochemistry.

In this section instead of analyzing specific phase diagrams we will adopt the viewpoint developed over the last five years by Miedema and co-workers in a very important series of papers.[54-57] Miedema has chosen to analyze the global problem of the systematics of the heats of formation of binaries formed from 27 transition and 26 simple metals. Thus he has introduced a global metric which is quite accurate for all 500 alloys as both solids and liquids. Because the model averages over so many systems it treats, in effect, only the isotropic part of the heat of formation, and not the anisotropic or structural part which is responsible for structural phase transitions. The theory is a chemical one in the sense that two variables are fixed for each element (106 elemental variables altogether) and thse are unaltered by the formation of chemical bonds. This assumption appears to be necessary and sufficient for calculating the isotropic part of ΔH_f.

How much information is contained in the phase diagrams studied by Miedema and co-workers? In general, far too much for a global model, and so although the model yields numerical values for ΔH_f, in practice, the variables have been adjusted to determine primarily the sign of ΔH_f as well as possible in approximately 500 binaries. (Actually the separation of ΔF into ΔH_f and ΔS is not trivial, so the model also contains certain qualitative rules[57] for establishing the sign of ΔH_f.) Although the data have been oversimplified, there are still 500 bits of information to be analyzed. This massive data base may be compared to 120 bits for the five crystal structures of 80 octet compounds, or 70 bits for six crystal structures of 50 suboctet compounds. It is therefore apparent that the successful separation of the fields "+" and "−" signs for ΔH_f in the dual-coordinate diagrams of Miedema, Boom, and deBoer is a remarkable accomplishment.

We now propose to trace this accomplishment through its final two stages and to show that the dual adjustable variables have fundamental quantum-mechanical significance. We recall that originally[54] for a rather small number of elements (about nine transition metals and 14 simple metals) values were given for the dual variables ϕ^* and n, interpreted as the atomic chemical potential and charge density at the edge of the (sphericalized or Wigner-Seitz) atomic cell. Shortly thereafter[55] the list was revised to include 27 transition metals and 15 simple metals. In both cases the values of ϕ^* were obtained from scattered and fragmentary experimental values of the work function ϕ. n was obtained from an empirical correlation between the molar volume V_m and the bulk modulus. It should be emphasized that such an intuitive, empirical approach is an excellent way of nucleating a global model.

The model formula for the heat of formation ΔH_f of an alloy $A_c B_{1-c}$ at this stage has the form[55]

$$\Delta H_f = f(c)[-Pe(\Delta\phi^*)^2 + Q(\Delta n)^2 - R\theta_s\theta_d], \qquad (20)$$

where $f(c)$ can be assigned the regular solution form $c(1-c)$. P, Q, and R are positive-valued constants. In (20) there is an attractive term associated with charge transfer $Pe(\Delta\phi^*)^2$, a repulsive term $Q(\Delta n)^2$ associated with charge-density mismatch, and an s-d correction term $R\theta_s\theta_d$ which is present for s-d pairs only ($\theta_s\theta_d = 1$) and absent otherwise ($\theta_s\theta_d = 0$).

The trial values[54] of ϕ^* and n were only partially successful, using (20), in predicting the sign of ΔH_f. This is shown in Fig. 20, which is repro-

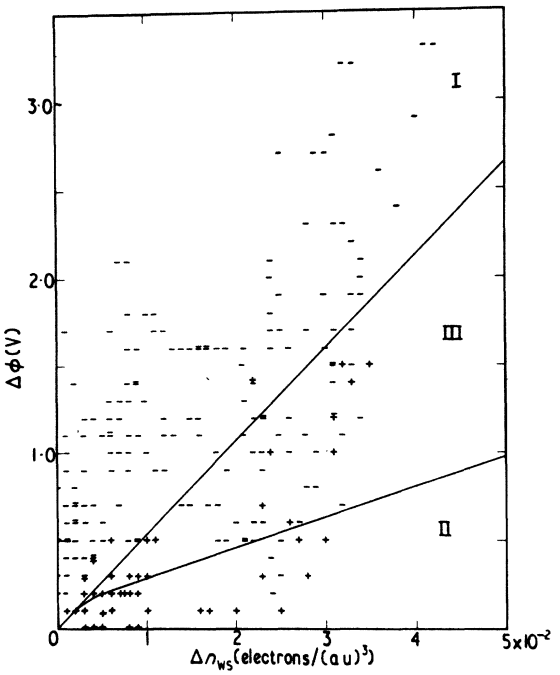

FIG. 20. Sign of ΔH_f for solid alloys correlated with differences in the work function $\Delta\phi$ and electronic charge density at the cell boundary Δn_{WS} for constituting metallic elements. Region I contains 107 negative and 4 positive signs while region II contains 37 positive signs and 2 negative signs. The results are from the early work of Miedema, deBoer, and Chatel (Ref. 54).

duced for the reader's convenience. The wedge region labelled III contains both "+" and "−" values, while region I contains 95% "−" values, and region II contains 95% "+" values. In view of the fact that (20) and the dual parameters (ϕ^*, n) were essentially guessed, the results shown in Fig. 20 are not unexpected. To examine the model further we took the postulated ϕ^* variables at this initial stage (i) and fitted them to the generalized orbital electronegativity (10) with $g(l)$ adjusted to give the best fit. The result was (simple metals only)

$$\tilde{\phi}_s^i = 3.69 + \frac{0.41}{r_0} + \frac{0.15}{r_1} - \frac{0.96}{r_2} \tag{21}$$

in eV. This result is unphysical in several ways: $|g(2)| \gg |g(1)|$ and $g(2) < 0$. However, there is a good fit in the sense that the rms error 0.12 eV.

The significance of our fitted values is brought out in Fig. 21, where we compare the thermochemical values with those fitted and predicted by (21). Although the general trends are similar, there are anomalies (notably Sn). However, the very unphysical value of $g(2)$ suggests either that ϕ^{*i} is unreliable or that the $\tilde{\phi}$ of our orbital shell model of electronegativity is not meaningful.

In view of our considerable success in examining structural properties, as detailed in the earlier sections of this paper, we were reluctant to accept the latter conclusion. We therefore decided to examine the most recent or final (f) set of variables[56] which are based on a much more extensive analysis of thermochemical data including liquid-metal alloys. Now there are changes in the formulas,

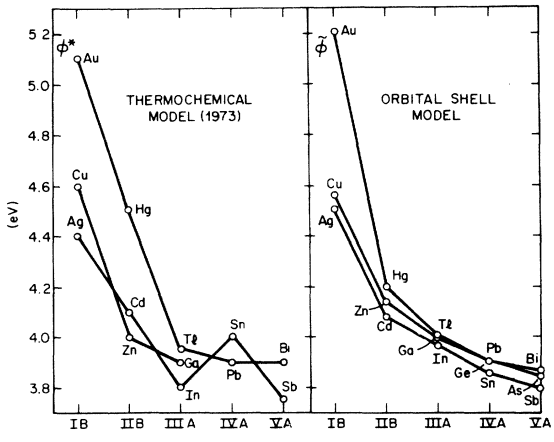

FIG. 21. Original (1973) work function parameters ϕ^* used by Miedema and co-workers (Ref. 55) in their thermochemical model for the heats of formation. Their results are compared to those obtained from an orbital shell model using an expansion in Block-Simons radii. Note the anomalous behavior of Sn in the thermochemical model. An orbital shell model fit to ϕ^* results in unphysical expansion coefficients.

notably $\Delta n^{1/3}$, i.e., the second variable has been adjusted more freely and is now found to correlate better with $[n(r_{WS})]^{1/3}$. Also there is a molar volume correction to the regular solution formula for $f(c)$, and some systematic dependence of R on Z_s (the valence of the simple metal) is identified. Most important to us, however, were further changes and augmentation of the variable list, which now includes 26 simple metals.

We therefore proceeded as before and made a similar fit to obtain

$$\tilde{\phi}_s^f = 0.62 + \frac{1.24}{r_0} + \frac{1.76}{r_1} + \frac{0.22}{r_2} \tag{22}$$

in eV, with an rms error of 0.12 eV again. This is a remarkable result. Now $g(l) > 0$ for all l, as it should be. Moreover, $g(2) \ll g(0), g(1)$, which is what we would expect for simple metals, and the coefficients indicate about 7% d hybridization, which is quite reasonable. Finally, the ratio of $g(1)/g(0)$ is pleasing. The metals studied span columns I (s) to V (s^2p^3) and therefore bearing in mind that we are concerned with electrons at the Fermi energy, one would expect (roughly) an average value of $g(1)/g(0)$ of about 1.5, close to fitted values. In fact, if we imagine that $g(2)$ has been borrowed mainly from $g(1)$, i.e., there is some p-d (dipole) hybridization in the crystal, then the ratio is very good indeed.

A comparison of ϕ_s^{*f} and $\tilde{\phi}_s^f$ as given by (22) is made in Fig. 22, again for the Cu, Ag, and Au periods. If one were to examine only the numerical values of ϕ_s^{*i} and compare them with φ_s^{*f}, the differences would seem rather small, compared, e.g., to the uncertainties of 0.4 eV which are not atypical of measured work functions ϕ. However, as we can see by comparison of Figs. 21 and 22, the *pattern* of ϕ^{*i} and $\tilde{\varphi}^i$ is totally different from

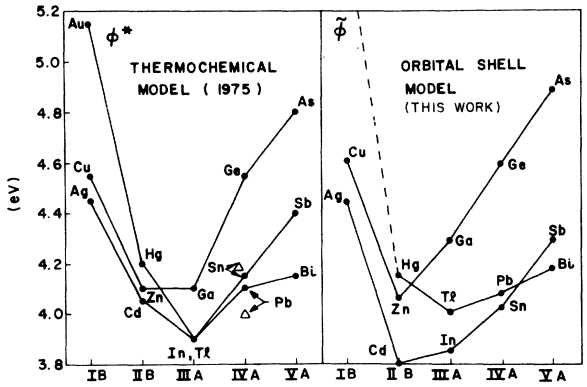

FIG. 22. Empirically adjusted work function parameters ϕ^* of the (1975) thermochemical model of Miedema and co-workers (Ref. 56). The results are compared to the orbital shell model parameters $\tilde{\phi}$.

the pattern of ϕ^{*f} and $\tilde{\phi}^f$. The first set of values decreases with Z, but the second set has a minimum at $Z=3$ (for ϕ^*) or at $Z=2$ (for $\tilde{\phi}$).

Because the agreement between ϕ^{*f} and $\tilde{\phi}^f$ is so good, and the physical results so reasonable, we could rest at this point and claim that our central goal—finding an orbital decomposition for, and justification of, the thermochemical variables—had been achieved. However, there is more to be said. The differences between ϕ^{*f} and $\tilde{\phi}^f$, although small, are not accidental; they are significant, and they shed light not so much on the thermochemical model but rather on the fundamental assumptions of the orbital shell model.

The central difference between ϕ^* and $\tilde{\phi}$ in Fig. 22 is that the range of values (for a given Z) spanned by $\tilde{\phi}$ is much greater than that spanned by ϕ^*. It seems very likely that the greater range of $\{\tilde{\phi}(Z)\}$ is a consequence of the simplifying assumption of the orbital shell model made at the outset, namely that the principal quantum number N is a good quantum number. Suppose we were to relax this assumption, and replace $r_l(N,Z)$ by (for example)

$$R_l(N,Z)=0.4r_l(N,Z)+0.3[r_l(N-1,Z)+r_l(N+1,Z)]. \quad (23)$$

We could then define $\tilde{\phi}(N,Z)$ in terms of $R_l(N,Z)$, and the end effect would be to reduce the range spanned by $\{\tilde{\phi}(Z)\}$ and bring it into better accord with the range of $\{\phi^*(Z)\}$; the ranges could be made nearly equal by suitably adjusting the broadening parameters in (23). However, we do not carry through this exercise because we feel that it would introduce further parameters but would provide no additional clarity.

There is a more penetrating way to analyze numerically the differences in Fig. 22. There is an oscillation in the I-B elements, with Cu and Au (periods IV and VI) having larger values of ϕ^* and $\tilde{\phi}$ than Ag (period V). The physical reason for this is well known: the tops of the bands of d electrons of Cu and Au lie about 2 eV below E_F, while that of Ag lies about 4 eV below E_F. Thus the d electrons of Cu and Au are much more polarizable than those of Ag, which enhances ϕ, ϕ^*, and $\tilde{\phi}$.

To us the most interesting feature of Fig. 22 is the extent to which this irregular feature of column I-B persists through columns II-A, III-A, and even IV-A, finally becoming small only in column V-A. Now the fact that Cu, Ag, and Au form solid solutions (α-brass or Hume-Rothery alloys) with all these elements is well known,[58] and preferentially each element dissolves in the I-B host of its own period. From Fig. 22 we would be inclined to say that it is the d-electron polarizability (even for Ge, Sn, and Pb!) and its regular contribution to (ϕ^*,n) that plays the most important role here.[59]

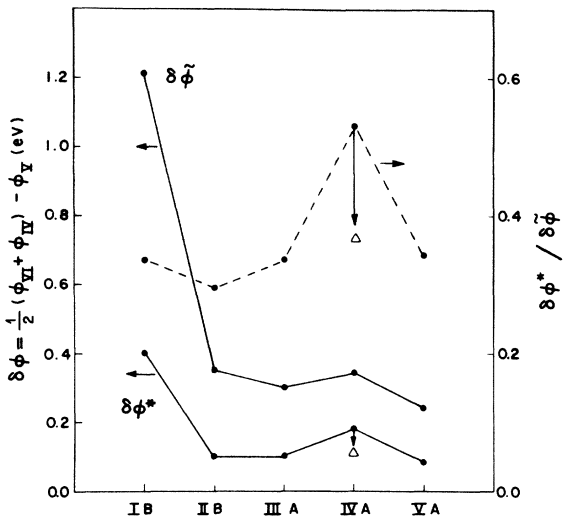

FIG. 23. Difference between the average of ϕ(IV) and ϕ(VI) and ϕ(V) as a function of Z in the thermochemical model (ϕ^*) (see text). Note the closely parallel behavior except for $Z=4$ which we attribute to small errors in ϕ^* for Sn and Pb. By modifying ϕ^* (as indicated by Δ) we bring the trends into agreement and obtain an improved fit to the Tl-Sn and Tl-Pb phase diagrams.

We can use the irregularity of the I-B sequence to calibrate the extent to which N is no longer a good quantum number in intermetallic alloys. Let us consider the quantity

$$\delta X(Z)\equiv\tfrac{1}{2}[X(VI,Z)+X(IV,Z)]-X(V,Z), \quad (24)$$

and substitute $X=\phi^{*f}$ and $X=\tilde{\phi}^f$. The results are shown in Fig. 23. The irregularity $\delta X(Z)$ is greatest for $Z=1$ (column I-B) and least for $Z=5$ (column V-A). However, the decrease is not monotonic, there being a small peak at $Z=4$ for both ϕ^* *and* $\tilde{\phi}$.

While it is obvious that $\delta\tilde{\phi}$ closely parallels $\delta\phi^*$, we also show the ratio $\delta\phi^*/\delta\tilde{\phi}$ in Fig. 23; this ratio has a value close to 0.35 ± 0.05 except for the case $Z=4$. To bring $\delta\phi^*(4)/\delta\tilde{\phi}(4)$ close to 0.35 as indicated by Δ in Fig. 23, we need only make the changes in ϕ^*(Sn) and ϕ^*(Pb) indicated by Δ in Fig. 22. Our largest recommended change is ϕ^*(Pb) from 4.10 to 4.00 eV, while ϕ^*(Sn) is changed from 4.15 to 4.18 eV. All other values of ϕ^{*f} appear to be consistent with a "blurred" orbital shell model.

If only $\frac{1}{3}$ of the shell structure irregularity survives not only the formation of energy bands but also the "statistical noise" of the 500 binary alloys studied in the global thermochemical model, why, one might ask, should we attach much significance to the orbital shell model? To answer this question,

let us look again at Fig. 22. Why is ϕ^*(Cd) $<\phi^*$(Zn) and ϕ^*(Hg)? Is this an artifact of Miedema's model, which contains (in addition to P, Q, and R) 106 elemental adjustable variables, or is it an intrinsic consequence of irregularities in the d core energy levels? What we show in Fig. 23 is that the irregularities of ϕ^* are indeed intrinsic. We believe that because of the very close agreement between ϕ^* and $\tilde{\phi}$ implied by $\delta\phi^*/\delta\tilde{\phi} = \text{const}$ that we are justified in believing that in general $\{\phi^{*f}\}$ is accurate to better than 0.04 eV.

Our success with fitting ϕ^* with a generalized orbital electronegativity relation (10) has encouraged us to look for a similar relation for $n^{1/3}$, the second thermochemical variable which appears in Miedema's later scheme. There is a strong internal correlation between ϕ^* and $n^{1/3}$, and as a result of this correlation it seems natural to fit $n^{1/3}$ again to a relation of the type (10). In addition, if we use relation (10) to describe $n^{1/3}$ we may explicitly demonstrate the rather large cancellation which occurs between the electronegativity and charge density terms in ΔH_f. The result (in Miedema's units) for $n^{1/3} = \psi^*$ is given by

$$\tilde{\psi} - \tilde{\psi}_0 = 0.318(\tilde{\phi} - \tilde{\phi}_0) - 0.041/r_p , \qquad (25)$$

where $\tilde{\phi}$ is given by (22) with $\tilde{\phi}_0 = 0.62$ and $\tilde{\psi}_0 = 0.21$. The rms error in (25) is 0.08. Because the range spanned by ϕ^* is about three times greater than that of ψ^*, this rms error is about twice as large as that in the fits to ϕ^*. Thus the following algebraic arguments are intended to be schematic rather than definitive.

To illustrate the large cancellation between ϕ^* and ψ^* we consider the most recent expression used for ΔH_f by Miedema:

$$\Delta H_f/P = -(\Delta\phi^*)^2 + (Q/P)(\Delta\psi^*)^2 - R\theta_d\theta_s/P \qquad (26)$$

(assuming nearly equal molar volumes). Q and P are constants, $Q/P = 9.4\ \text{V}^2/(\text{density units})^{2/3}$. Assuming $\theta_d\theta_s = 0$ we substitute (22) and (25) into (26) and obtain

$$\Delta H_f/P = -0.25\Delta\tilde{\phi}[0.20\Delta\tilde{\phi} + \Delta(1/r_p)] . \qquad (27)$$

This expression explicitly exhibits the large cancellation between the ϕ^* and ψ^* contributions which is characteristic of the heats of formation. The terms in P and Q have cancelled by 95%. The result implies that "first-principles" calculations using local pseudopotentials, phase shifts (muffin tins), or any of the other simplifications commonly employed in energy-band calculations of bulk or surface properties are unlikely to yield results sufficiently accurate to be of thermochemical interest.

According to (22) and (25) the central difference between $\tilde{\phi}$ and $\tilde{\psi}$ is an additional p-shell contribution to $\tilde{\psi}$. Because the p-shell contribution is small $[\delta g(1) \ll g(1)]$, it is natural to interpret this as the average effect of a higher-order multipole contribution to the charge in the boundary energy[60] at polyhedral cellular interfaces when intermetallic compounds are formed. The average isotropic or spherical contribution to $\Delta\tilde{\phi}$ favors $\Delta H_f < 0$, but kinetic energies are more strongly affected by the polyhedral terms which emphasize ψ^* and favor $\Delta H_f > 0$. The situation in metallic compounds is quite different from molecules. In molecules, low-order multipoles give large kinetic energies and stability is possible, in general, only through covalent bonding.

While our expression for $\tilde{\psi}$ in (25) is of significance for demonstrating the rather large cancellations between the $\Delta\phi^*$ and $\Delta\psi^*$ terms in ΔH_f, the $\tilde{\psi}$ values are unsatisfactory because the rms error from ψ^* is rather large. In order to remedy this situation we tried numerous combinations of r_l with little success. However, we were able to obtain an accurate fit to ψ^*, involving only a few parameters, provided we employed the isotropic radii, r_m, where we take $r_m = V_m^{1/3}$.[56] In general, we expect the atomic charge density to have the asymptotic form $n(r) \sim \exp(-\alpha r_m^{\beta})/r$ and thus we attempted the expansion

$$\tilde{\psi} = \tilde{\psi}_0 + \exp(-\alpha r_m^{\beta}) \sum_l \frac{g(l)}{r_l} . \qquad (28)$$

We found that the best fit was obtained with $\beta = 2$, $\alpha = 0.096$, $g(0) = 0.45$, $g(1) = 0.50$, and $g(2) = 0.40$. The rms error for (28) was 0.04 or a twofold improvement over our previous expression for ψ^*. The relative values of $g(l)$ are stable for large changes in β indicating that they are probably of physical significance.

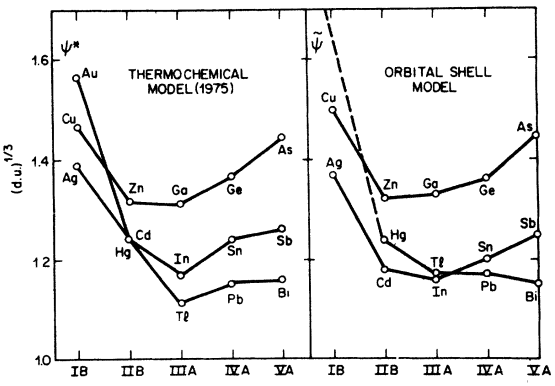

FIG. 24. Comparison of Miedema's most recent thermochemical parameters ψ^* with values predicted by the orbital shell model according to Eq. (28), which includes both ion-core and atomic size factors. $(\psi^*)^3$ is given in density units (d.u.) as in Ref. 56.

TABLE VI. Electronegativity and charge-density parameters (ϕ^*, ψ^*) as defined by Miedema and co-workers (Refs. 54–56) for simple metals. Miedema's parameters are compared to the analogous parameters ($\tilde{\phi}, \tilde{\psi}$) as defined by the orbital shell model [Eqs. (22) and (28)]. Au was not used to fix the expansion coefficients in the orbital shell model and we tabulate it for completeness only.

Element	ψ^*	$\tilde{\psi}$	ϕ^*	$\tilde{\phi}$
Li	0.98	0.99	2.85	2.92
Na	0.82	0.83	2.70	2.62
K	0.65	0.68	2.25	2.21
Rb	0.60	0.65	2.10	2.12
Cs	0.55	0.61	1.95	1.99
Be	1.60	1.56	4.20	4.55
Mg	1.17	1.09	3.45	3.36
Ca	0.91	0.90	2.55	2.72
Sr	0.84	0.81	2.40	2.50
Ba	0.81	0.76	2.32	2.30
Al	1.39	1.33	4.20	4.03
Si	1.50	1.53	4.70	4.64
Cu	1.47	1.50	4.55	4.61
Ag	1.39	1.37	4.45	4.44
Au	1.57	(1.87)	5.15	(6.69)
Zn	1.32	1.32	4.10	4.06
Cd	1.24	1.18	4.05	3.76
Hg	1.24	1.24	4.20	4.15
Ga	1.31	1.33	4.10	4.29
In	1.17	1.16	3.90	3.85
Tl	1.12	1.17	3.90	4.01
Sn	1.24	1.20	4.15	4.02
Pb	1.15	1.17	4.10	4.08
As	1.44	1.49	4.80	4.89
Sb	1.26	1.25	4.40	4.30
Bi	1.16	1.15	4.15	4.18
Ge	1.37	1.46	4.55	4.59

A comparison between the orbital shell model results and the thermochemical model results for ψ is displayed in Fig. 24. In contrast to the results for $\tilde{\phi}$, we note the anomalous behavior of $\tilde{\psi}$ for the I-*B* (Cu, Ag, Au) column does not penetrate beyond the III-*B* column. In this sense the orbital shell effects for $\tilde{\psi}$ seem to be reduced as compared to $\tilde{\phi}$. Otherwise, the behavior of $\tilde{\psi}$ resembles that of $\tilde{\phi}$ leading to the large cancellation in ΔH_f.

In summary, the orbital-shell-model parameters ($\tilde{\psi}, \tilde{\phi}$) are compiled along with the thermochemical model parameters (ψ^*, ϕ^*) in Table VI for the convenience of the reader.

VII. CONCLUSIONS

In this paper we have attempted to illustrate how suitable combinations of Bloch-Simons radii may be used to construct chemical coordinates. Our purpose in constructing these coordinates is to develop intuition and insight with respect to the relationship between chemical composition and crystal structure. As indicated in Sec. I, the prediction of crystal structures is a most difficult problem: one which involves energy differences which are too small to be calculated using our present quantum mechanical framework. We have proceeded, therefore, not from a "first-principles" approach, which at this time appears fruitless, but rather attempted to separate schematically the structures using the diagrammatic approaches of Mooser-Pearson and Phillips–Van Vechten.

As a first attempt, we have restricted our efforts to include only simple binary compounds of the form $A^N B^{P-N}$, where $P=8$ and $2<P<6$. Although these groups have been briefly examined before by St. John and Bloch,[10] and Machlin, Chow, and Phillips,[15] respectively, we have extended their results to include the noble metals (Cu, Ag, and Au) and discussed their approaches in more detail. We noted the extremely important result that using the *same* combinations of radii we were able to separate both the octet ($P=8$) and suboctet crystal groups. In addition, we noted the anomalous placement of structures in a St. John–Bloch diagram, in certain cases, was indicative of special or unusual crystalline behavior (e.g., CuF, CaAg, and RbAu).

While in most cases we found the original definitions of Bloch and Simons to be satisfactory, we did extend their results to include variations in the $l=2$ radii down the columns of the Periodic Table. This difference can be significant in defining electronegativity scales for certain elements as, for example, Si and Ge. We also expanded their results to include the noble metals (Cu, Ag, and Au) and to include the heavy halogens. Finally we generalized the electronegativity scale of St. John and Bloch and noted that such scales may be calibrated by recent thermochemical models.

Further, we noted specific advantages of the St. John–Bloch coordinates over other coordinate schemes. Unlike the MP coordinates, the SB coordinates are completely quantum mechanical in nature and are not of digital form. Thus SB coordinates vary smoothly across the rows and down the columns of the Periodic Table. They are also adaptable to a wide range of simple binary structures. This is not true, for example, of the PVV coordinates. These latter coordinates, while very successful, are restricted in their applicability to sp^3, or tetrahedrally coordinated, binary compounds. Nevertheless, in some cases we were able to find correlations between the SB coordinates and the other schemes. As an example we found the SB coordinate r_σ, correlated very well with Pauling's electronegativity and to a lesser ex-

tent with the PVV parameter, C.

In addition to the great success of obtaining a nearly exact separation of the octet and suboctet binary crystal structures, we have also obtained striking correlations of the Bloch-Simons radii with internal crystal parameters involving uniaxial distortions occurring in the wurtzite and $A^{II}B^{IV}C_2^V$ chalcopyrite structures. Specifically, we were able to account for the c/a ratios in wurtzites by using the SB r_σ coordinate alone. This result should be contrasted with the work of Lawaetz.[47] Lawaetz used a complicated chemical coordinate involving the formal valence of the cation, the plasma energy and the Phillips ionic energy gap C. Our results are comparable to his yet we employ on the r_s and r_p orbital radii of Bloch and Simons. In the case of the chalcopyrite structures we also obtained a satisfactory correlation between the c/a ratios and a combination of orbital radii. Unfortunately, this correlation failed for cases in which relativistic effects become large.

Another aspect examined in the paper was the melting point behavior of approximately 40 suboctet binary compounds. These compounds are more amenable to a simple analysis than the octets as they do not contain anions which tend to associate in the liquid phase. In order to compare the effectiveness of the SB coordinates over the MP coordinates we expanded the melting temperatures T_f to second order in (r_σ, r_π) and $(\bar{n}, \Delta X)$. The expansion coefficients were fixed by experiment. The MP coordinate expansion was very poor in describing T_f; the fit was accurate ~30% and the expansion coefficients ill defined. Most of the difficulty could be traced to the digitalized form of $\bar{n}$, and the incapacity of $(\bar{n}, \Delta X)$ to make fine distinctions between the binaries. On the other hand, the SB coordinates yielded a satisfactory description of the melting point behavior. The accuracy was ~15%, a considerable improvement over the MP results.

Encouraged by the success of the orbital radii to account for the melting points of the suboctets, we used the radii to analyze the recent thermochemical model of Miedema and co-workers.[54-56] Miedema has developed classical thermochemical parameters (ϕ^*, ψ^*) which he found were capable of predicting the sign of the heat of formation for several hundred liquid and solid binary alloy systems. In an examination of his parameters we found that they could be expressed in terms of orbitally dependent ionic radii. Significantly, we found that the irregularity of the core shell structure could be identified in his parameters and we were able to demonstrate a large cancellation occurring between the charge transfer and kinetic energy contributions to ΔH_f.

All the results of the present paper seem to depend on the precise form of the Simons pseudopotential, Eq. (1). For each l this pseudopotential contains one adjustable parameter $\hat{l}$, which is determined from the quantum defect $\delta_{nl} = \hat{l} - l$. We are aware, however, that the r^{-2} term in the Simons pseudopotential can be refined by modifying its functional form at large r and by including a second adjustable parameter.[61] With two adjustable parameters one can fit both E_{nl} and P_{nl}, the value of r corresponding to the radial maximum of the Hartree-Fock wave function of the appropriate hydrogenic ion. At present, unfortunately, we have values of P_{nl} only for elements from the first period.[61] When a complete set of P_{nl} become available, it will be necessary to refine the Simons-Bloch orbital radii r. The question is, how much will this change our answers? Will the empirical regularities presented here still be valid?

Our expectation is that the changes in r_l produced by refining (1) will be largely multiplicative, corresponding to nearly constant scaling factors. Thus we suppose that refinement of the pseudopotential will not alter the results of this paper greatly, as long as the refined pseudopotential contains an r^{-2} "hard-core" term for small r even for s states. (Most pseudopotentials used in early work[18] were chosen for reasons of computational convenience to be of the Ashcroft "empty-core" type.) In these cases there will always be classical turning points which can be used to define l-dependent ion-core radii similar to the Simons-Bloch radii used here.

In this paper we have attempted primarily to expand the data base to which quantum structural pseudopotential theories can be applied. The most sophisticated pseudopotential calculations at present employ l-dependent pseudopotentials, fitted either to experimental band structures[62,63] or to energies and wave-function maxima of neutral atoms or hydrogenic ions.[64] However, for the most part these calculations are carried out in an isolated manner which does not make manifest the regularities in core properties (especially core turning points) as a function of l, Z, and N which are immediately evident in Figs. 1–3 and Table I. We hope that the connections between structural regularities and hard-core nonlocal pseudopotentials discovered by this and other recent work will encourage a systematic global approach to these problems.

APPENDIX A: "ANOMALOUS Au"

We have noted in the discussion of Fig. 15 in Sec. IV that MgAu has a melting point which is

500 °C higher than that of ZnAu (or, e.g., CdAu) and which is 500° higher than the value predicted by fitting to all other suboctet intermetallic compounds (rms deviation 140 °C). The very high melting point cannot be explained by the large difference in chemical potential between Mg and Au, for other compounds with equally large differences in chemical potential are described adequately.

We believe that an important difference between MgAu and ZnAu lies in the presence of a very loosely filled d shell on Au, a d core level on Zn that is only ~10 eV below the Fermi energy on Zn, and no d core states in Mg. In the crystal the Au d states can "expand" into the Mg cells more than into the Zn cells. This effect is qualitatively included in the r_d values of Table I for Mg and Zn, but not in r_σ and r_π. In any case, such a d-d effect lies outside the framework of our s-p coordinates or Miedema's coordinates (which lump together s, p, and d effects). In some ways the anomalously high melting point of MgAu may be attributed to p-d hybridization, which is described in the Miedema model by the third term on the right-hand side of Eq. (26), especially if Au is regarded as a special element which lies halfway between Cu and Ag, one the one hand, and Pb and Pt on the other, in terms of its Miedema coordinates $(\phi^*, n^{1/3})$.

[1](a) W.B. Pearson, *Handbook of Lattice Spacings and Structures of Metals* (Pergamon, New York, 1967), Vol. 2; (b) *The Crystal Chemistry and Physics of Metals and Alloys* (Wiley, New York, 1972).

[2]M. Hansen, *Constitution of Binary Alloys* (McGraw-Hill, New York, 1958); R. P. Elliott, *ibid.*, First Suppl., 1965; F. A. Shunk, *ibid.*, Second Suppl , 1969.

[3]E. Parthe, *Crystal Chemistry of Tetrahedral Structures* (Gordon and Breach, New York, 1970).

[4]*Treatise on Solid State Chemistry*, edited by N. B. Hannay (Plenum, New York, 1973–1977), Vols. 1–7.

[5]L. Pauling, *The Nature of the Chemical Bond*, 3rd. ed. (Cornell, Ithaca, N. Y., 1960).

[6]J. C. Phillips, Rev. Mod. Phys. 42, 317 (1970); also Ref. 4, Chap. 1, Vol. I.

[7]L. S. Darken and R. W. Gurry, *Physical Chemistry of Metals* (McGraw-Hill, New York, 1953); J. T. Waber *et al.*, Trans. Metall. Soc. AIME 227, 717 (1963).

[8]E. Mooser and W. B. Pearson, Acta Crystallogr. 12, 1015 (1959).

[9]J. A. Van Vechten, Phys. Rev. 182, 891 (1969); 187, 1007 (1969); Phys. Rev. B 7, 1479 (1973).

[10]J. St. John and A. N. Bloch, Phys. Rev. Lett. 33, 1095 (1974).

[11]G. Simons, J. Chem. Phys. 55, 756 (1971); 60, 645 (1974).

[12]G. Simons, Chem. Phys. Lett. 12, 404 (1971); 18, 315 (1973).

[13]G. Simons and A. N. Bloch, Phys. Rev. B 7, 2754 (1973).

[14]A. N. Bloch and G Simons, J. Am. Chem. Soc. 94, 8611 (1972).

[15]E. S. Machlin, T. P. Chow, and J. C. Phillips, Phys. Rev. Lett. 38, 1292 (1977).

[16]J. C. Phillips, Solid State Commun. 22, 549 (1977).

[17]E. Fues, Ann. Phys. (Leipz.) 80, 367 (1926).

[18]See, for example, M. L. Cohen and V. Heine, Solid State Phys. 24, 37 (1970), and references therein.

[19]C. E. Moore, *Atomic Energy Levels*, Natl. Bur. Stds. (U.S.) Circ. (U.S. GPO, Washington, D.C., 1952).

[20]W. Gordy and W. J. O. Thomas, J. Chem. Phys. 24, 439 (1956).

[21]A. R. Miedema, J. Less-Common Met. 32, 117 (1973); A. R. Miedema, R. Boom, and F. R. DeBoer, *ibid.* 41, 283 (1975).

[22]R. Boom, F. R. deBoer, and A. R. Miedema, J. Less-Common Met. 46, 271 (1976).

[23]J. C. Phillips, *Bonds and Bands in Semiconductors* (Academic, New York, 1973).

[24]J. A. Van Vechten, Phys. Rev. 182, 891 (1969).

[25]H. Jagodzinski, Neues Jahrbach Mineral. Monatsh. 10, 49 (1954); H. Jagodzinski and H. Arnold, *Proceedings of the Conference on Silicon Carbide* (Pergamon, New York, 1960), p. 141.

[26]N. A. Goryunova, *The Chemistry of Diamond-Like Semiconductors* (Chapman and Hall, London, 1965), pp. 42–57.

[27]H. Mittendorf, Z. Phys. 183, 113 (1965).

[28]W. G. Wyckoff, *Crystal Structure* (Interscience, New York, 1963), Vol. I, pp. 110 and 189.

[29]F. Ebert and H. Woitneck, Z. Anorg. Chem. 210, 269 (1933).

[30]M. Barber, J. W. Linnett, and N. M. Taylor, J. Chem. Soc. 3323 (1961).

[31]Von H. Von Wartenberg, Z. Anorg. Chem. 241, 381 (1939).

[32]W. B. Pearson, in Ref. 1b, expecially pp 568ff, 367, and 214ff.

[33]R. Kiessling, Acta Chem. Scand. 3, 595 (1949).

[34]P. I. Kripyakevich, Soc. Phys.-Crystallogr. 6, 626 (1961).

[35]See, W. Reiger and E. Parthe, Acta Crystallogr. 22, 919 (1967), and references therein.

[36]E. N. Lebedeva, V. V. Karonik, N. Cherkashina, and N. M. Kagan, Zh. Prikl. Khim. 43, 763 (1970).

[37]H. M. Huang and T. L. Liu, Phys. Lett. A 46, 295 (1973).

[38]A. Baldereschi and F. Meloni, Helv. Phys. Acta 49, 160 (1976).

[39]W. E. Spicer, A. N. Sommer, and J. G. White, Phys. Rev. 115, 57 (1959).

[40]J. A. Van Vechten, Phys. Rev. Lett. 29, 769 (1972).

[41]F. A. Lindemann, Z. Phys. 11, 609 (1910).

[42]J. M. Ziman, *Principles of the Theory of Solids* (Cambridge U.P., Cambridge, England, 1964), p. 63.

[43]Melting points were obtained from Ref. 2 and W. G. Moffatt, *Binary Phase Diagrams Handbook* (General Electric, Schenectady, N.Y., 1976).

[44]See Ref. 1b, p. 74.

[45]R. C. Hanson, J. R. Halberg, and C. Schwab, Appl.

Phys. Lett. 21, 490 (1972).
[46]J. C. Phillips, J. Electrochem. Soc. 123, 934 (1976).
[47]P. Lawaetz, Phys. Rev. B 5, 4039 (1972).
[48]P. Lawaetz, Phys.Rev. Lett. 26, 697 (1971).
[49]For a review of the chalcopyrite structures and properties, see A. S. Borshehevskii, N. A. Goryunova, F. P. Kesamanly, and D. N. Nadledev. Phys. Status Solidi 21, 91 (1967).
[50]J. C. Phillips, J. Phys. Chem. Solids 35, 1205 (1974).
[51]S. C. Abrahams and J. L. Bernstein, J. Chem. Phys. 55, 796 (1971).
[52]J. Shay and J. L. Wernick, *Ternary Chalcopyrite Semiconductors* (Pergamon, New York, 1975), p. 85.
[53]L. Kaufmann, in *Phase Stability of Metals and Alloys*, edited by P. S. Rudman (McGraw-Hill, New York, 1967).
[54]A. R. Miedema, F. R. deBoer, and P. F. DeChatel, J. Phys. F 3, 1558 (1973).
[55]A. R. Miedema, J. Less-Common Met. 32, 117 (1973).
[56]A. R. Miedema, R. Boom, and F. R. deBoer, J. Less-Common. Met. 41, 283 (1975); R. Boom, F. R. deBoer, and A. R. Miedema, *ibid.* 45, 237 (1966); 46, 271 (1967).
[57]For an overview, see A. R. Miedema, Philips Tech. Rev. 36, 217 (1976).
[58]N. F. Mott and H. Jones, *Theory of the Properties of Metals and Alloys* (Oxford U.P., Oxford, England, 1936).
[59]Optical data showing the influence of local bonds in α-phase noble metal alloys on d-band widths have been reported by D. Beaglehole and M. Wihl, Solid State Commun. 13, 427 (1973).
[60]D. G. Pettifor, Comm. Phys. 1, 141 (1976); J. Phys. F 7, 4 (1977).
[61]A. Baldereschi (private communication); M. L. Cohen (private communication).
[62]K. C. Pandey and J. C. Phillips, Phys. Rev. B 9, 1552 (1974).
[63]J. R. Chelikowsky and M. L. Cohen, Phys. Rev. B 14, 556 (1976).
[64]J. R. Chelikowsky, Solid State Commun. 22, 351 (1977); S. G. Louie, K. M. Ho, J. R. Chelikowsky, and M. L. Cohen, Phys. Rev. Lett. 37, 1289 (1976).